Available online at www.sciencedirect.com

ScienceDirect

Geochimica et Cosmochimica Acta 215 (2017) 51–75

Geochimica et Cosmochimica Acta

www.elsevier.com/locate/gca

Evidence for a chondritic impactor, evaporation-condensation effects and melting of the Precambrian basement beneath the 'target' Deccan basalts at Lonar crater, India

Rahul Das Gupta [a,1], Anupam Banerjee [a,1], Steven Goderis [b,c], Philippe Claeys [b], Frank Vanhaecke [c], Ramananda Chakrabarti [a,*]

[a] Centre for Earth Sciences, Indian Institute of Science, Bangalore, 560012, India
[b] Vrije Universiteit Brussel, Analytical-, Environmental- & Geo-Chemistry, Pleinlaan 2, 1050 Brussels, Belgium
[c] Ghent University, Department of Analytical Chemistry, Campus Sterre, Krijgslaan, 281 – S12, 9000 Ghent, Belgium

Received 14 February 2017; accepted in revised form 11 July 2017; Available online 19 July 2017

Abstract

The ~1.88 km diameter Lonar impact crater formed ~570 ka ago and is an almost circular depression hosted entirely in the Poladpur suite of the ~65 Ma old basalts of the Deccan Traps. To understand the effects of impact cratering on basaltic targets, commonly found on the surfaces of inner Solar System planetary bodies, major and trace element concentrations as well as Nd and Sr isotopic compositions were determined on a suite of selected samples composed of: basalts, a red bole sample, which is a product of basalt alteration, impact breccia, and impact glasses, either in the form of spherules (<1 mm in diameter) or non-spherical impact glasses (>1 mm and <1 cm). These data include the first highly siderophile element (HSE) concentrations for the Lonar spherules. The chemical index of alteration (CIA) values for the basalts and impact breccia (36.4–42.7) are low while the red bole sample shows a high CIA value (55.6 in the acid-leached sample), consistent with its origin by aqueous alteration of the basalts. The Lonar spherules are classified into two main groups based on their CIA values. Most spherules show low CIA values (Group 1: 34.7–40.5) overlapping with the basalts and impact breccia, while seven spherules show significantly higher CIA values (Group 2: >43.0). The Group 1 spherules are further subdivided into Groups 1a and 1b, with Group 1a spherules showing higher Ni and mostly higher Cr compared to the Group 1b spherules. Iridium and Cr concentrations of the spherules are consistent with the admixture of 1–8 wt% of a chondritic impactor to the basaltic target rocks. The impactor contribution is most prominent in the Group 1a and Group 2 spherules, which show higher Ni/Co, Ni/Cr and Cr/Co ratios compared to the target basalts. In contrast, the Group 1b spherules show major and trace element compositions that overlap with those of the impact breccia and are characterized by high EF_{Th} (Enrichment Factor for Th defined as the Nb-normalized concentration of Th relative to that of the average basalt) as well as fractionated $La/Sm_{(N)}$, and higher large ion lithophile element (LILE) concentrations compared to the basalts. The relatively more radiogenic Sr and less radiogenic Nd isotopic composition of the impact breccia and non-spherical impact glasses compared to the target basalts are consistent with melting and mixing of the Precambrian basement beneath the Deccan basalt with up to 15 wt% contribution of the basement to these samples. Variations in the moderately siderophile element (MSE) concentration ratios of the impact breccia as well as all the spherules are best explained by contributions from three components – a chondritic impactor, the basaltic target rocks at Lonar and the basement underlying the Deccan basalts. The large variations in concentrations of

* Corresponding author.
E-mail addresses: ramananda@ceas.iisc.ernet.in, ramananda@gmail.com (R. Chakrabarti).
[1] Equal contribution from authors.

http://dx.doi.org/10.1016/j.gca.2017.07.022
0016-7037/© 2017 Elsevier Ltd. All rights reserved.

volatile elements like Zn and Cu and correlated variations of EF_{Cu}-EF_{Zn}, EF_{Pb}-EF_{Zn}, EF_{K}-EF_{Zn} and EF_{Na}-EF_{Zn}, particularly in the Group 1a spherules, are best explained by evaporation-condensation effects during impact. While most spherules, irrespective of their general major and trace element composition, show a loss in volatile elements (e.g., Zn and Cu) relative to the target basalts, some spherules, mainly of Group 1, display enrichments in these elements that are interpreted to reflect the unique preservation of volatile-rich vapour condensates resulting from geochemical fractionation in a vertical direction within the vapour cloud.
© 2017 Elsevier Ltd. All rights reserved.

Keywords: Lonar impact crater; Impact spherules; Chondritic impactor; Basement melting; Impact volatilization and condensation

1. INTRODUCTION

Impact craters are ubiquitous features in the Solar System. Given that the inner Solar System planetary bodies and some of the Jovian satellites have basaltic crusts (Walker et al., 1979), impact craters on basaltic rocks are a common feature on planetary bodies. On Earth, impact craters on a purely basaltic target are rare. One example is the ~1.88 km diameter simple crater at Lonar in Maharashtra, India (Fig. 1) which is now a saline water lake (Fredriksson et al., 1973; Kieffer et al., 1976; Fudali et al., 1980). Isotopic studies indicate that the basalts around Lonar correlate with the Poladpur suite, one of the mid-section volcano-stratigraphic units of the Deccan Traps (Chakrabarti and Basu, 2006). Another example is the Logancha crater, which is thought to be formed on the Siberian flood basalts (Feldman et al., 1983; Masaitis, 1999). However, the Logancha crater is difficult to access due to permanent ice cover. Hence, in the context of planetary analogue studies, the Lonar crater presents a unique opportunity to study impact cratering on basaltic surfaces.

Early studies considered the Lonar crater to be a volcanic crater (Gilbert, 1896; La Touche and Christie, 1912; Nandy and Deo, 1961). However, the principal reasons to infer an impact-origin for the Lonar crater are: (i) the presence of a single crater amidst the vast Deccan Traps, (ii) the unlikely scenario of flood basalts erupting by formation of a crater, and (iii) the apparent young age, as inferred from the thin sediment cover (Lafond and Dietz, 1964). The lack of Ni and Co enrichments in soils, lake sediments, brines, plants, and spring water at Lonar prompted Venkatesh (1965) to suggest that the Lonar crater is non-meteoritic in origin. However, Hawkes (1967) argued against the approach of Venkatesh (1965) by showing that even at the Meteor crater in Arizona, which is clearly of meteoritic origin, plants and soils do not show any enrichment in Ni concentrations. The impact-origin of the Lonar crater was confirmed by the discovery of "glassy objects" (Nayak, 1972) and shatter cones and shock metamorphic features in drill-core samples (Fredriksson et al., 1973). Later studies revealed the occurrence of basalts with different degrees of shock metamorphism at Lonar, validating an impact origin (Kieffer et al., 1976). A smaller depression, 700 m north of the Lonar crater, known as the Ambar crater or Little Lonar (Fig. 1), is considered to be a second impact crater (Fredriksson et al., 1973; Master, 1999).

Initial attempts to date the formation of the Lonar crater yielded recent ages. A study implementing thermoluminescence to the Lonar impact glasses resulted in an age of 52,000 ± 6000 years (Sengupta et al., 1997) whereas fission track dating yielded an age of 15 ± 13 ka (Storzer and Koeberl, 2004). However, the above-mentioned techniques are prone to resetting by alteration and younger thermal events (cf., Storzer and Koeberl, 2004; Jourdan et al., 2011). More recently, Ar-Ar dating of melt rock samples have constrained the formation age of the Lonar crater at 570 ± 47 ka (Jourdan et al., 2011), which is currently the preferred age of formation.

Early geochemical studies suggested that the Lonar impact glasses are enriched in the alkali elements Na and K (Nayak, 1972), as well as in Si (Murali et al., 1987) compared to the target basalt. In contrast, other studies showed that the impact glasses are chemically similar to the target basalts, with possible depletion in Na, which was interpreted as impact-induced volatile loss (Fredriksson et al., 1973; Stroube et al., 1978). The originally observed enrichments in Na and Si were thus suggested to be of anthropogenic origin (Fudali and Fredriksson, 1992). However, enrichments in Na, K and other large-ion lithophile elements (LILE, including K, Rb, Cs, Sr, Ba) relative to the target basalts have been observed in the impactites in more recent geochemical studies too (Osae et al., 2005; Chakrabarti and Basu, 2006; Son and Koeberl, 2007; Misra et al., 2009). Preferential melting of plagioclase in the target basalt upon impact has been suggested as one of the possible mechanisms to enrich the LILE concentration of the impact-melts (Misra and Newsom, 2011; Ray et al., 2017).

Measurements of Nd-Sr-Pb isotopic compositions of impact breccia suggested that the Archaean basement underlying the Deccan basalts at Lonar melted upon impact and contributed to the composition of the Lonar impact breccia (Chakrabarti and Basu, 2006). However, this basement melting model has been questioned. First, an anthropogenic influence on the impact breccia samples (man-made bricks) analysed by Chakrabarti and Basu (2006) has been suggested (Misra, 2006; Deenadayalan et al., 2009; Misra et al., 2009; Maloof et al., 2010). Secondly, Son and Koeberl (2007) pointed out that the excavation depth of the Lonar crater, estimated by these authors to be 150–300 m based on the diameter of the crater, is two to three times less than the expected thickness of the Deccan basalts at Lonar, rendering the melting of the basement unlikely. However, Nd and Sr isotopic compositions of impactite samples collected independently by multiple research groups (Chakrabarti et al., 2006; Schulz et al.,

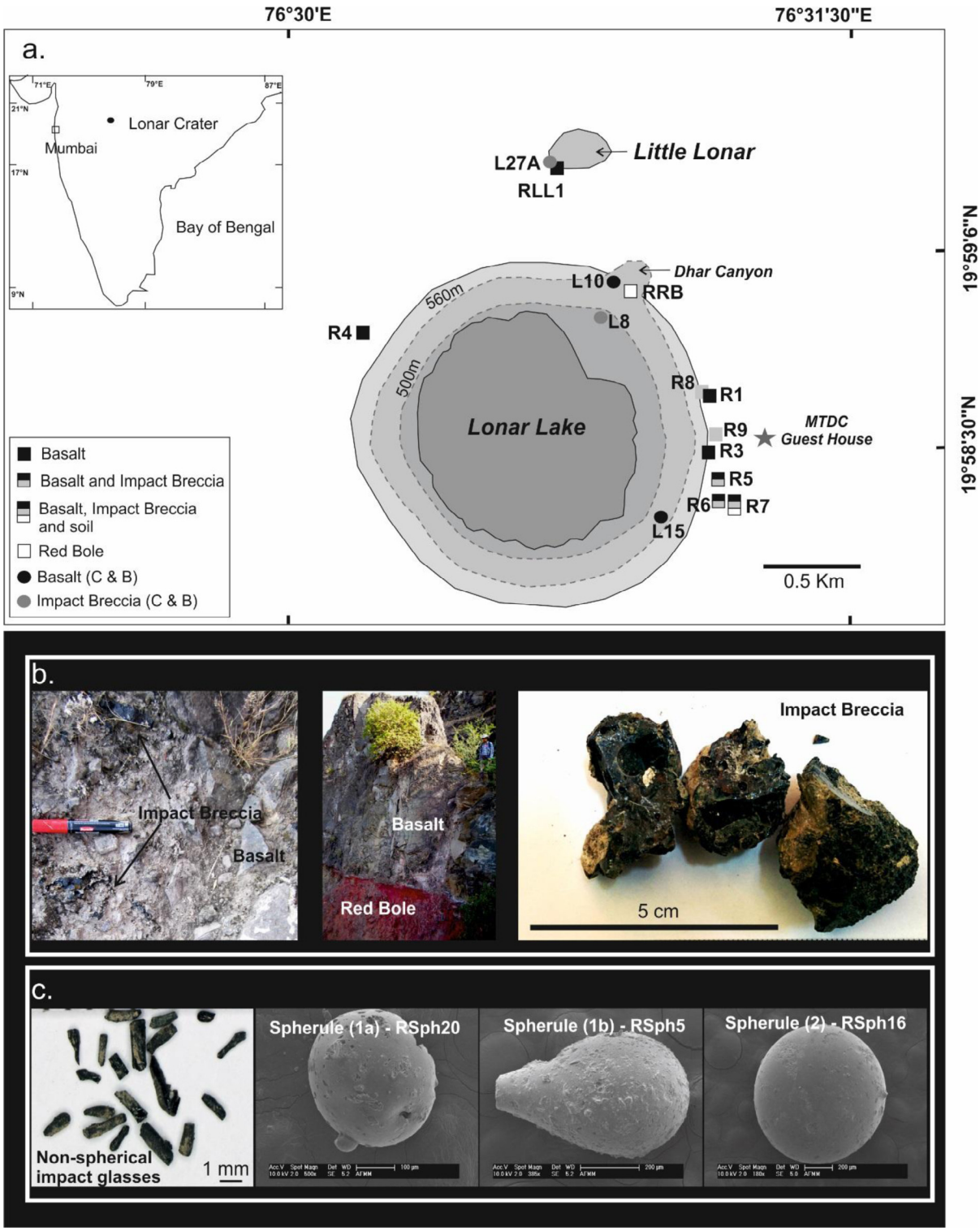

Fig. 1. (a) Location of the Lonar crater in India and a simplified map of the Lonar crater showing sampling locations of the basalts, impact breccia, soil sample from which the spherules and non-spherical impact glasses were extracted, and red bole. The basalts L10, L15 and the impact breccia samples L8 and L27A (circles, C&B) were collected as part of an earlier study (Chakrabarti and Basu, 2006). (b) Field photographs of in-situ samples of the basalt, impact breccia and red bole at Lonar as well as hand specimen samples of the impact breccia. (c) Image of the aerodynamically-shaped non-spherical impact glasses and back-scattered electron (BSE) images of three different geochemical types of spherules, all separated from the soil sample at R7.

2016) overlap with the composition of the impact breccia samples of Chakrabarti and Basu (2006) and concur with the basement melting model (Chakrabarti and Basu, 2006). Borehole drilling at Killari, in the eastern part of the Deccan Traps (~280 km from Lonar), has revealed the presence of Archean granites and gneisses beneath ~340 m thick basalts (Gupta et al., 1999) while the lower estimate of the depth of the Lonar crater by Chakrabarti and Basu (2006) is 350 m, which is consistent with the possibility of basement melting at Lonar.

Meteoritic impactor fragments are not preserved at Lonar. Early geochemical attempts to detect impactor signatures from the impact rocks yielded mostly inconclusive results (Venkatesh, 1965; Hawkes, 1967). The lack of excesses in highly siderophile element (HSE, such as Ir or Pt) as well as moderately siderophile element (MSE, including Ni and Co) concentrations were explained by a lack or limited contribution of the impactor to the melt rock composition (Morgan, 1978; Osae et al., 2005). Based on the lack of HSE excesses, an Ir-poor iron meteorite impactor was proposed for the Lonar crater (Osae et al., 2005). Using MSE concentration ratios in Lonar impact spherules (Misra et al., 2009), as well as HSE concentration ratios and $^{187}Os/^{188}Os$ in impact glasses and impact melt rocks (Schulz et al., 2016), a chondritic impactor has been suggested for Lonar. Based on MSE concentration ratios in Lonar spherules, this projectile contribution was specified to derive from an EH-type chondrite (Ray et al., 2017), whereas Cr isotopic measurements of Lonar impact glasses suggest a carbonaceous chondritic impactor (Koeberl et al., 2017).

In an effort to understand the geochemical and isotopic effects of impact cratering on basaltic targets, we report major and multi-trace element concentrations of target basalts and a suite of impactites, as well as Nd and Sr isotopic compositions of selected basalts and impactites. We also report geochemical and Nd and Sr isotopic compositions of a red bole sample, formed by basalt alteration, from Lonar. We evaluate the geochemical and isotopic composition of the impactites in terms of melting of the basaltic target and the basement, mixing of the impactor, target basalts and the basement, evaporation-condensation processes accompanying the impact event, and post-formation aqueous alteration of the samples.

2. SAMPLES AND ANALYTICAL METHODS

Samples of Deccan (target) basalts and impact breccia as well as soil samples excavated from a shallow pit were collected from several locations around the Lonar crater, within a few hundred meters from the crater rim, and Little Lonar in 2013 (Fig. 1a). In this study, the term impact breccia is used for bulk samples showing clear evidence of melting and shock and is based on arguments presented in Chakrabarti and Basu (2006) (Fig. 1b). Aerodynamically shaped impact glasses were hand-picked from the soil samples collected from the south-eastern rim of the crater (Fig. 1a). The soil samples were sorted using locally-made nylon sieves with aperture sizes of 1 mm and 0.5 mm. The two finer fractions contained impact glasses, which were hand-picked using sharpened wooden picks under a binocular stereomicroscope at the Centre for Earth Sciences (CEaS), Indian Institute of Science (IISc). Among the impact glasses, spherical-shaped impact glasses with <1 mm diameter are referred to as spherules in the present study, while elongate and dumbbell-shaped impact glasses with longest dimensions greater than 1 mm but less than 1 cm are referred to as non-spherical impact glasses (Fig. 1c). All the products of impact, which include the impact breccia, spherules and non-spherical impact glasses, are referred to as impactites. A total of seven basalt samples and five impact breccia samples were collected. The collected samples were fresh and did not show any visual signs of alteration. In addition to the above-mentioned samples, we re-analysed two basalt samples (L10, L15) and two impact breccia samples (L8, L27A) collected as part of an earlier study (Chakrabarti and Basu, 2006). A sample of a clay-rich intra-basaltic horizon derived from weathering of the Deccan basalt, defined as red bole (Wilkins et al., 1994) (Fig. 1b), was collected from the Dhar canyon at Lonar (Fig. 1a).

The bulk rock samples were gently crushed to cm-sized chips using a rock hammer. Several grams of these chips were cleaned using 18.2 MΩ cm water by ultra-sonication and air dried, and subsequently crushed using an agate mortar and pestle. Samples L10, L15, L8 and L27A (Chakrabarti and Basu, 2006) were already in powdered form, whereas the red bole sample was directly crushed using an agate mortar and pestle. Approximately 25 mg of the powdered samples were dissolved in 15 ml screw-cap Teflon vials using a combination of Suprapur HF (Merck) and Emsure brand HNO_3 and HCl acids (Merck, ACS, Reag. PhEur), the latter two acids were previously further purified using a Savillex DST-1000 sub boiling still, according to established protocols (Banerjee et al., 2016). After dissolution, the samples were taken up in 100 ml of 2% HNO_3 in pre-cleaned 125 ml HDPE bottles to achieve a dilution factor of ~4000. All samples were processed in a class 100 laminar flow work area hosted in a class 10,000 clean room at the CEaS, IISc. The United States Geological Survey (USGS) rock standards BHVO-2 (Hawaiian basalt), BCR-2 (Columbia River basalt), and AGV-2 (andesite) were processed in the same way as the rock samples.

Element concentrations were measured using a Thermo Scientific X-Series II quadrupole inductively coupled plasma mass spectrometer (ICPMS) at the CEaS, IISc. An internal standard mixture with 10 ppb of Be, In, Cs and Bi was added to all blanks, samples and standards "on-line" to correct for instrumental drift. Sample solutions were introduced from a CETAC ASX-520 auto-sampler, actively transported through a PFA nebulizer with a flow rate of 100 μL/min using a peristaltic pump, to an ESI-PC3 Peltier-cooled spray chamber. Barring elements prone to spectral overlap from Ar-containing molecular ions (masses between 40 amu and 86 amu) for which the collision/reaction cell mode (using a mixture of H_2 and He gases introduced at 7 ml/min) was used, the concentrations of most elements were determined in the standard mode. The instrument was tuned to reduce the CeO^+/Ce^+ ratio to <2% to minimize oxide-related interferences. The raw

counts for all elements were corrected for the contribution from acid blanks and converted to concentrations using USGS rock standards BHVO-2 and BCR-2, which were used as calibration standards. The accuracy of the data was tested by analyzing USGS rock standards AGV-2 and BHVO-2, interspersed with the samples. The experimental results agree within 2% with the corresponding reference values for the rare earth elements (REEs) and within 5% for the other elements (Supplementary Table A.1). Internal precision (%RSD, relative standard deviation), based on three repeat measurements is better than 2%. Our laboratory acid blanks are <1 ppt for the REEs, <1 ppb for all other elements analyzed barring some major elements like Na for which it is <10 ppb.

A preliminary size-sorting of the spherules was done using a stereomicroscope and 35 spherules with the least number of surface pits were chosen for geochemical characterization. Due to the difficulty in weighing the spherules, elemental concentration measurements of the spherules using solution-based ICPMS were not performed. Fresh-looking spherules were selected for elemental analyses using laser ablation (LA)-ICPMS at Ghent University (UGent). These spherules range between ~133 and 672 μm in diameter (Table 2). Concentrations of major and trace elements in thirty-five selected Lonar spherules (Table 2) were determined using a 193 nm ArF^* excimer-based Analyte G2 laser ablation system (Teledyne CETAC Technologies, Omaha, USA) coupled to an Element XR (Thermo Fisher Scientific, Bremen, Germany) sector-field ICPMS unit. Analysis was performed via repeated (2–5 times) laser drilling using a laser spot size of 50 μm in diameter, a laser dwell time of 20 s, a repetition rate of 40 Hz, and a beam energy density of 3.51 J/cm^2 on the spherule surface. The spherules and reference materials were mounted in a standard HELEX 2 double-volume ablation cell. The He carrier gas (0.5 L/min) was mixed with Ar make-up gas downstream of the ablation cell, and introduced into the ICPMS unit, operated at low mass resolution. Semi-cold plasma conditions (800 W RF power) were used to reduce Ar-based interferences. Precise and accurate trace element concentration data were obtained based on external calibration, using matrix-matched MPI-DING glass reference materials GOR 128-G, StHS6/80-G, GOR 132-G, ATHO-G, ML3B-G, T1-G, and KL2-G and total oxide normalization to 100 wt.%. Following this procedure, precise and accurate major, minor and trace element concentrations were obtained for USGS glass reference materials BCR-2G, BIR-1G and BHVO-2G (Supplementary Table A.1). Based on the analyses of the reference materials, the reproducibility for the elements measured are typically 5–10 %RSD depending on the concentration (Wittmann et al., 2013; Van Roosbroek et al., 2015). However, the HSE Re, Ir, Pt and Au show precisions of 10–20 % RSD because of their occurrence in ppb-level concentrations only (Table 2). The limits of detection (LOD) for Re, Ir, Pt, Au are 1, 1, 0.3 and 3 ppb, respectively.

Neodymium and Sr isotope ratio measurements were carried out using a Thermo Scientific Triton Plus thermal ionization mass spectrometer (TIMS) at CEaS, IISc, using a laboratory protocol described in Banerjee et al. (2016). Selected basalts, impact breccia, non-spherical impact glasses, spherules and the red bole were dissolved using ultrapure HF, HNO_3 and HCl acids. Spherules and non-spherical impact glasses with relatively less pitted surfaces, were ultrasonicated using 18.2 MΩ cm water to remove any surface contamination prior to dissolution for isotopic measurements. Owing to their small size and weight, fourteen non-spherical impact glasses were dissolved together and processed for Sr and Nd isotopic analysis. Similarly, fifteen relatively large spherules with an average diameter of ~500 μm (labelled as "Spherules-large") were dissolved together, while seventeen smaller spherules of ~250 μm diameter (labelled as "Spherules-small") were dissolved together and only Sr isotope ratio data was successfully obtained for these two sets of spherules. Due to the small sample size and weight, these spherules and non-spherical impact glasses could not be analyzed for elemental concentrations. Strontium and Nd were isolated from the samples using ion-exchange chromatography. Primary separation was done using BioRad AG50W X8 (100–200 mesh) resin, from which Sr was eluted in 3 M HCl, while the REEs and Ba were eluted in 6 M HCl. The Sr fraction was further cleaned using the same resin in a smaller column. From the eluted fraction containing the REEs and Ba, Nd was separated using BioRad AG50W X8 (200–400 mesh) resin with 0.2 M 2-hydroxyisobutyric acid at a pH of 4.495. A final purification of the Nd fraction was achieved using the same resin but in a smaller column using 6 M HCl. The procedural blanks for Nd and Sr are measured to be <400 pg. Strontium was loaded using ~0.7 M H_3PO_4 on degassed and oxidised Ta filaments and analyzed using a single filament assembly, while Nd was loaded in ~0.03 M H_3PO_4 on degassed zone-refined Re filaments and analyzed using a double filament assembly. Instrumental mass fractionation during $^{87}Sr/^{86}Sr$ and $^{143}Nd/^{144}Nd$ isotope ratio measurements was corrected by internal normalization using $^{86}Sr/^{88}Sr = 0.1194$ and $^{146}Nd/^{144}Nd = 0.7219$, respectively. Uncertainties in the $^{143}Nd/^{144}Nd$ ratios for the samples correspond to 0.000003 ($2s_{mean}$, internal precision). The JNdi-1 Nd isotopic standard analyzed during this study yielded $^{143}Nd/^{144}Nd = 0.512118 \pm 8$ (2SD, n = 4). Uncertainties in the measured $^{87}Sr/^{86}Sr$ are less than 0.000009 ($2s_{mean}$, internal precision). The NIST SRM 987 Sr isotopic standard analyzed during this study yielded $^{87}Sr/^{86}Sr = 0.710265 \pm 10$ (2SD, n = 5).

3. RESULTS

Concentrations of major and trace elements in nine basalts, seven impact breccia and one red bole were determined using solution-based ICPMS (Table 1). We have analysed the bulk sample as well as an acetic acid-leached sample of the red bole. Among these samples, the basalts L10 and L15 and impact breccia samples L8 and L27A were characterized in an earlier study (Chakrabarti and Basu, 2006) and re-analyzed for comparison in this study. Elemental concentrations of these four samples are consistent with earlier measurements. Concentrations of Si were not determined as our dissolution procedure uses HF acid, the use of which results in loss of Si by volatile-loss of SiF_4.

Table 1
Major and trace element concentrations determined by ICPMS after acid digestion of target basalts, impact breccia and red bole from the Lonar crater.

Sample#	Rock type	CIA	Na (wt%)	Mg (wt%)	Al (wt%)	K (wt%)	Ca (wt%)	Ti (wt%)	Fe (wt%)	Mn (wt%)	P (ppm)	Li (ppm)	Sc (ppm)	V (ppm)	Cr (ppm)	Co (ppm)	Ni (ppm)	Cu (ppm)	Zn (ppm)	Rb (ppm)	Sr (ppm)	Y (ppm)	Zr (ppm)	Nb (ppm)	Ba (ppm)
R1	Basalt	36.4	1.65	3.5	7.2	0.48	7.6	1.21	10.0	0.128	732	6.8	36	430	109	118	79	121	85	16.4	207	29	127	9.2	96
R3	Basalt	36.9	1.81	3.2	6.7	0.51	6.6	1.52	11.1	0.147	910	7.9	35	435	35	118	52	138	99	18.8	213	37	271	11.7	119
R4	Basalt	37.1	1.82	3.2	6.8	0.29	6.9	1.53	11.0	0.164	1025	5.8	35	440	62	119	53	121	108	8.6	251	35	184	12.2	167
R5	Basalt	36.8	1.69	3.5	6.8	0.138	7.2	1.55	11.7	0.186	1063	8.5	36	430	33	129	53	158	115	4.2	225	36	174	12.1	73
R6	Basalt	37.2	1.85	3.3	6.9	0.50	6.8	1.52	11.5	0.155	827	7.1	35	435	34	124	53	156	99	16.6	216	35	159	11.1	121
R7	Basalt	36.8	1.84	3.4	6.9	0.25	7.1	1.50	11.1	0.21	880	6.0	35	427	34	122	53	119	93	3.8	230	35	165	10.5	125
RLL1	Basalt	36.7	1.84	3.2	6.8	0.50	6.9	1.43	11.0	0.27	973	6.8	35	422	34	123	54	144	108	16.8	219	36	163	10.1	130
L10	Basalt	36.4	1.67	4.1	7.3	0.148	8.0	1.22	10.4	0.147	789	5.4	36	386	112	131	86	129	90	2.4	214	30	131	9.0	76
L15	Basalt	36.4	1.78	3.4	6.7	0.51	6.9	1.51	11.8	0.162	912	7.2	36	432	36	129	55	160	106	18.4	209	36	162	10.2	119
R5b	Impact breccia	38.0	1.68	3.1	7.1	0.53	6.8	1.37	10.2	0.153	1016	8.8	34	382	70	113	53	137	104	18.5	248	35	176	11.1	193
R6b	Impact breccia	38.0	1.82	3.1	7.1	0.56	6.8	1.42	10.4	0.154	957	9.1	34	390	65	112	52	124	96	19.5	252	36	178	11.4	231
R7b	Impact breccia	38.6	1.72	3.2	7.2	0.51	6.8	1.38	10.0	0.150	834	8.8	33	389	80	111	58	103	83	17.9	247	34	285	11.2	198
R8	Impact breccia	36.4	1.66	3.4	6.7	0.37	7.0	1.41	10.3	0.151	385	8.7	35	398	100	130	136	117	101	13.6	243	37	179	11.7	187
R9	Impact breccia	37.0	1.58	3.1	6.8	0.38	7.1	1.26	9.3	0.139	446	8.5	34	368	101	116	70	96	84	14.8	233	33	158	10.6	142
L8	Impact breccia	42.7	1.17	3.9	7.3	0.67	5.9	1.16	9.7	0.151	1522	10.3	32	320	65	112	56	106	74	24	236	33	155	10.0	141
L27A	Impact breccia	40.0	1.02	3.0	6.5	0.95	5.8	1.66	10.5	0.167	3935	9.7	33	415	102	120	75	116	108	24	198	30	149	11.6	179
RRB	Red Bole (bulk)		0.23	2.4	4.2	0.39	11.7	0.54	6.4	0.042	21	15.3	21	70	47	68	54	147	55	24	160	18.8	125	6.0	60
RRB-L*	Red Bole leached	55.6	0.30	3.0	5.8	0.52	3.0	0.80	9.3	0.039	0.087	20	26	171	64	40	77	333	80	34	84	13.8	118	9.6	64

Sample#	Rock type	La (ppm)	Ce (ppm)	Pr (ppm)	Nd (ppm)	Sm (ppm)	Eu (ppm)	Gd (ppm)	Tb (ppm)	Dy (ppm)	Ho (ppm)	Er (ppm)	Tm (ppm)	Yb (ppm)	Lu (ppm)	Hf (ppm)	Ta (ppm)	Pb (ppm)	Th (ppm)	U (ppm)
R1	Basalt	9.9	24.8	3.61	17.0	4.87	1.64	5.5	0.89	5.5	1.11	2.86	0.409	2.56	0.362	3.3	0.75	1.73	1.39	0.30
R3	Basalt	14.1	33.9	4.88	22.6	6.2	2.02	6.9	1.11	6.9	1.40	3.58	0.52	3.24	0.456	4.2	0.88	2.1	2.1	0.48
R4	Basalt	16.1	38.1	5.3	24.2	6.4	2.11	7.0	1.10	6.7	1.34	3.39	0.477	3.00	0.415	4.6	0.84	3.3	2.8	0.49
R5	Basalt	13.5	34.3	4.94	23.1	6.4	2.08	7.1	1.14	6.9	1.40	3.60	0.51	3.18	0.444	4.4	0.89	2.7	2.2	0.45
R6	Basalt	13.4	32.6	4.67	21.7	6.0	1.99	6.7	1.08	6.6	1.35	3.47	0.490	3.09	0.432	4.2	0.81	2.5	2.0	0.49
R7	Basalt	13.4	33.2	4.72	22.1	6.0	2.01	6.7	1.08	6.7	1.35	3.46	0.493	3.09	0.431	4.2	0.73	2.4	2.0	0.42
RLL1	Basalt	13.3	33.2	4.70	21.8	6.1	2.00	6.7	1.08	6.6	1.36	3.50	0.497	3.11	0.443	4.2	0.63	2.8	2.0	0.49
L10	Basalt	10.0	25.2	3.68	17.5	4.98	1.69	5.6	0.90	5.6	1.14	2.94	0.421	2.65	0.376	3.4	0.71	1.67	1.42	0.29
L15	Basalt	13.3	32.3	4.63	21.5	6.0	1.95	6.6	1.07	6.5	1.34	3.47	0.50	3.10	0.437	4.1	0.66	2.3	2.0	0.48
R5b	Impact breccia	19.0	42.7	5.6	24.8	6.4	1.99	6.8	1.07	6.4	1.33	3.39	0.488	3.04	0.432	4.4	0.75	4.1	3.0	0.58
R6b	Impact breccia	19.3	43.6	5.8	25.3	6.5	2.03	7.0	1.09	6.6	1.35	3.49	0.494	3.12	0.436	4.5	0.83	4.4	3.0	0.58
R7b	Impact breccia	18.2	41.0	5.5	24.0	6.2	1.95	6.7	1.06	6.4	1.31	3.35	0.479	3.01	0.424	4.3	0.82	4.0	2.9	0.65
R8	Impact breccia	16.0	37.6	5.4	23.9	6.6	2.29	7.2	1.29	7.0	1.58	3.69	0.70	3.29	0.830	4.2	0.97	3.3	2.4	0.59
R9	Impact breccia	15.1	34.8	4.71	21.2	5.6	1.79	6.2	0.97	6.0	1.23	3.13	0.444	2.78	0.391	3.8	0.79	3.4	2.6	0.55
L8	Impact breccia	15.6	37.0	4.96	22.2	5.8	1.90	6.4	1.01	6.1	1.25	3.24	0.467	2.92	0.417	4.0	0.75	1.62	2.9	0.64
L27A	Impact breccia	12.8	30.2	4.15	18.8	5.0	1.62	5.6	0.90	5.6	1.13	2.91	0.420	2.62	0.373	3.8	0.75	20	2.6	0.52
RRB	Red Bole (bulk)	8.2	16.0	2.51	11.0	2.88	0.91	3.22	0.53	3.29	0.69	1.77	0.253	1.56	0.219	1.92	0.36	4.6	2.0	0.58
RRB-L*	Red Bole leached	8.3	15.8	2.10	8.3	2.02	0.63	2.26	0.380	2.50	0.53	1.40	0.205	1.28	0.179	2.8	0.62	6.6	2.7	0.32

Data for chondrites used for normalization are from Taylor and McLennan (1985)

Sample#	Rock type	$La/Sm_{(N)}$	Ni/Cr	Ni/Co	Cr/Co	Fe/Cr
R1	Basalt	1.28	0.73	0.67	0.92	919
R3	Basalt	1.43	1.50	0.44	0.29	3225
R4	Basalt	1.57	0.86	0.45	0.52	1776
R5	Basalt	1.32	1.61	0.41	0.26	3526
R6	Basalt	1.40	1.57	0.43	0.27	3377
R7	Basalt	1.41	1.54	0.43	0.28	3238
RLL1	Basalt	1.38	1.59	0.44	0.28	3228
L10	Basalt	1.27	0.77	0.66	0.85	926
L15	Basalt	1.39	1.54	0.43	0.28	3288
R5b	Impact breccia	1.88	0.76	0.47	0.62	1466
R6b	Impact breccia	1.87	0.80	0.47	0.58	1595
R7b	Impact breccia	1.85	0.73	0.52	0.72	1254
R8	Impact breccia	1.52	1.36	1.05	0.77	1025
R9	Impact breccia	1.71	0.69	0.60	0.87	918
L8	Impact breccia	1.70	0.86	0.50	0.58	1484
L27A	Impact breccia	1.60	0.73	0.62	0.85	1028
RRB	Red Bole (bulk)	1.80	1.16	0.79	0.68	1365
RRB-L*	Red Bole leached	2.59	1.19	1.93	1.62	1445

* Red bole sample was leached with acetic acid to remove carbonates. CIA value determined for the residue after leaching.

With the exception of samples R1 and L10, the basalt samples show elemental concentrations that are broadly similar to one another (Table 1). The concentrations in the impact breccia samples broadly overlap with those of the basalts while the red bole shows clear differences (Table 1). For the spherules, the concentrations of major and trace elements were determined using LA-ICPMS (Table 2). Significant compositional variability exists among the spherules (Table 2). The non-spherical impact glasses were not measured for their trace element concentrations. Details of the compositional variations in the Lonar samples are discussed in the following sections.

3.1. Chemical index of alteration

The basalts and impact breccia samples do not show any visual signs of alteration. While most spherules show smooth surfaces with a glassy appearance, back-scattered electron (BSE) images of some spherules exhibit apparent surface alteration in the form of pits and roughness of the surface (Fig. 1c). Given the preservation state of the samples, especially the spherules, values for the chemical index of alteration (CIA) of all the samples were calculated according to Nesbitt and Young (1982), as:

$$CIA = [Al_2O_3/(Al_2O_3 + CaO + Na_2O + K_2O)] * 100 \quad (1)$$

The target basalts at Lonar show the lowest CIA values, which range from 36.4 to 37.2. The impact breccia samples show overlapping CIA (36.4–42.7) with the basalts. Impact breccia samples L8 and L27A show slightly high values of 42.7 and 40.0, respectively (Table 1). The CIA value of the bulk red bole sample is 20.4, while that of the red bole sample leached with 2% acetic acid is 55.6 (Table 1). The spherules show a relatively large range in CIA values ranging from 34.7 to 65.6 (Table 2) and are sub-divided into Group 1 ($n = 28$), with CIA values ranging from 34.7 to 40.5, and Group 2 ($n = 7$), which shows CIA values greater than 43.0. The CIA values of the Group 1 spherules overlap with that of the basalts and impact breccia samples, whereas the CIA values of the Group 2 spherules overlap with that of the leached red bole sample (Fig. 2). The Group 1 spherules are further divided into Groups 1a and 1b based on their MSE concentrations and ratios, as discussed in Section 3.3.

3.2. Enrichment factors (EF) of elements

Niobium-normalized concentration of an element compared to the Nb-normalized concentration of the same element in the average basalt at Lonar is defined as the "enrichment factor" (EF). The selection of Nb is based on its fluid immobile (cf., Banerjee et al., 2016) as well as refractory behaviour (50% T_C of 1559 K; Lodders, 2003). Based on our measurements, the average Nb concentration in the Lonar basalt is 10.7 ± 2.4 ppm (2SD) (Nb data from Table 1). The EF of several elements in the basalts, impact breccia and spherules are plotted in Fig. 3. By definition, the EF of the average basalt has a value of unity for all elements. Values of EF_{Na}, EF_{Ca} and EF_K for the spherules and impact breccia mostly fall below unity with Group 2

Table 2
Major and trace element concentrations of spherules from the Lonar crater determined by LA-ICPMS.

Sample#	Type	Diameter	CIA	Na_2O (wt%)	MgO (wt%)	Al_2O_3 (wt%)	SiO_2 (wt%)	P_2O_5 (wt%)	K_2O (wt%)	CaO (wt%)	TiO_2 (wt%)	MnO (wt%)	FeO_T (wt%)	Li (ppm)	Sc (ppm)	V (ppm)	Cr (ppm)	Co (ppm)	Ni (ppm)	Cu (ppm)	Zn (ppm)	Rb (ppm)
R-Sph-2	1a	274	37.83	1.75	7.3	12.6	49	0.199	0.28	9.7	2.3	0.24	16.6	6.4	35	377	441	114	1386	223	112	9.9
R-Sph-3	1a	398	39.31	1.74	7.1	13.2	47	0.184	0.28	9.4	2.4	0.24	17.8	8.6	36	371	393	122	1612	255	126	11.2
R-Sph-4	1a	429	38.72	1.55	7.5	12.9	48	0.125	0.22	9.7	2.4	0.25	16.9	7.0	34	321	389	120	1478	166	84	7.6
R-Sph-7	1a	347	39.29	2.3	4.5	13.9	48	0.29	0.62	9.4	4.3	0.197	16.5	8.3	32	511	99	58	205	412	173	13.7
R-Sph-8	1a	224	38.41	2.4	5.9	13.5	52	0.092	0.41	9.5	2.4	0.20	13.6	6.4	36	387	145	67	499	209	76	9.7
R-Sph-15	1a	233	40.52	3.2	4.0	16.1	52	0.36	0.56	9.8	1.9	0.157	11.2	11.2	23	312	144	46	233	363	179	12.3
R-Sph-17	1a	200	37.36	1.89	6.0	13.6	49	0.178	0.36	10.6	2.7	0.22	15.7	8.8	39	455	261	80	600	229	113	13.0
R-Sph-18	1a	297	34.71	2.0	6.0	13.1	49	0.192	0.46	11.5	2.7	0.20	14.5	7.0	44	417	130	58	270	191	111	12.9
R-Sph-19	1a	293	39.75	1.28	8.2	14.8	46	0.126	0.22	11.0	2.9	0.25	15.3	7.4	43	343	231	85	995	146	67	9.2
R-Sph-20	1a	329	38.87	1.41	7.5	13.4	48	0.055	0.192	10.2	2.6	0.24	16.5	5.7	39	321	315	117	1423	111	48	6.1
R-Sph-21	1a	420	38.41	1.86	7.8	13.2	47	0.22	0.31	9.8	2.4	0.25	16.6	7.2	36	385	514	128	1778	234	122	10.9
R-Sph-23	1a	235	37.42	1.47	9.1	13.3	44	0.165	0.22	10.7	2.6	0.25	17.8	6.9	41	325	485	134	1570	169	101	7.6
R-Sph-24	1a	272	39.57	1.90	6.8	13.9	47	0.197	0.30	9.8	2.6	0.24	16.9	8.5	40	400	288	93	976	257	113	11.9
R-Sph-26	1a	230	38.64	1.81	7.3	13.1	48	0.20	0.30	9.7	2.4	0.24	16.8	8.3	36	363	433	122	1672	217	120	12.0
R-Sph-27	1a	296	37.31	2.5	5.6	13.9	49	0.32	0.52	10.2	2.5	0.22	14.9	7.4	40	444	129	67	355	374	212	15.2
R-Sph-30	1a	159	39.67	1.75	6.0	13.4	50	0.032	0.23	9.5	2.7	0.23	16.2	7.2	36	354	90	64	273	127	43	5.3
R-Sph-33	1a	158	36.86	1.51	7.5	13.4	47	0.097	0.192	11.1	2.6	0.25	16.1	6.3	8	331	164	94	980	139	61	5.2
R-Sph-35	1a	161	35.98	2.1	8.3	11.9	47	0.30	0.32	9.6	2.3	0.25	17.2	7.0	34	411	685	140	1855	253	134	10.9
R-Sph-5	1b	672	36.76	2.1	5.6	12.9	52	0.26	0.57	10.0	2.4	0.21	13.6	6.8	40	376	86	50	58	202	122	16.9
R-Sph-6	1b	497	38.05	2.3	5.5	14.3	51	0.193	0.50	10.5	2.3	0.195	13.4	8.4	37	370	101	50	64	193	112	14.9
R-Sph-9	1b	385	35.75	1.75	6.6	12.7	48	0.197	0.46	10.7	2.8	0.24	16.0	6.2	50	411	78	55	75	168	123	13.6
R-Sph-12	1b	246	39.36	2.1	5.0	15.2	50	0.25	0.67	10.5	2.5	0.20	13.5	9.5	39	372	56	44	48	213	118	24
R-Sph-13	1b	231	38.87	2.4	6.0	14.3	50	0.25	0.75	9.7	2.3	0.22	13.7	9.2	35	407	94	48	60	197	120	19.0
R-Sph-14	1b	393	38.46	2.2	5.6	14.9	51	0.123	0.47	10.9	2.2	0.194	12.0	5.9	37	374	106	45	72	122	56	13.5
R-Sph-22	1b	252	36.92	2.2	5.6	14.0	51	0.20	0.53	10.8	2.4	0.20	13.1	8.0	41	378	98	51	56	195	122	14.5
R-Sph-29	1b	145	39.13	2.3	5.2	15.2	51	0.22	0.51	10.6	2.4	0.181	12.2	6.1	36	353	90	46	59	187	114	14.2
R-Sph-32	1b	133	39.10	2.3	5.3	15.3	50	0.25	0.64	10.7	2.3	0.20	13.3	8.0	36	371	65	46	51	220	120	19.4
R-Sph-34	1b	199	36.85	2.3	5.3	13.1	52	0.21	0.56	10.0	2.1	0.193	13.9	8.1	32	387	121	52	68	201	126	16.6
R-Sph-1	2	367	43.47	0.83	7.3	16.4	46	0.043	0.129	10.9	2.8	0.24	15.6	4.2	41	262	151	67	509	91	43	2.8
R-Sph-10	2	246	52.11	1.11	5.0	15.6	51	0.076	0.34	6.7	2.9	0.26	16.9	13.1	40	353	193	103	1002	210	76	21
R-Sph-11	2	204	49.32	0.71	5.7	25	38	0.136	0.156	13.6	3.4	0.190	12.0	6.9	74	299	251	74	1000	179	76	8.2
R-Sph-16	2	254	46.23	0.57	6.5	14.5	50	0.0128	0.10	8.7	2.8	0.26	15.9	5.8	38	172	124	90	550	24	32	3.8
R-Sph-25	2	296	56.08	0.71	3.3	14.9	56	0.106	1.28	5.0	2.6	0.175	15.8	9.5	32	262	208	43	215	253	104	35
R-Sph-28	2	327	51.55	1.14	4.4	16.3	50	0.079	0.32	7.2	3.2	0.28	16.8	9.4	45	322	136	82	539	88	46	15.3
R-Sph-31	2	230	65.62	0.67	3.5	17.7	52	0.076	0.51	4.2	3.3	0.27	17.4	23.4	42	370	178	87	551	183	108	43

Sample#	Type	Sr (ppm)	Y (ppm)	Zr (ppm)	Nb (ppm)	Ba (ppm)	La (ppm)	Ce (ppm)	Pr (ppm)	Nd (ppm)	Sm (ppm)	Eu (ppm)	Gd (ppm)	Tb (ppm)	Dy (ppm)	Ho (ppm)	Er (ppm)	Tm (ppm)	Yb (ppm)	Lu (ppm)	Hf (ppm)
R-Sph-2	1a	212	32	151	11.1	133	13.9	33.2	4.70	22.4	6.1	1.91	6.6	0.96	6.4	1.25	3.04	0.387	2.69	0.381	3.8
R-Sph-3	1a	205	33	162	12.4	142	13.6	33.8	4.97	24.5	6.9	2.01	7.5	1.13	6.8	1.31	3.43	0.400	3.02	0.471	4.4
R-Sph-4	1a	218	33	152	11.0	143	13.7	34.1	5.1	22.4	6.4	2.03	6.8	1.11	6.0	1.29	3.02	0.471	2.80	0.438	4.0
R-Sph-7	1a	252	30	169	13.0	144	15.2	33.3	4.79	22.0	6.9	2.12	6.6	0.93	6.1	1.16	2.85	0.483	2.74	0.378	4.2

R-Sph-8	1a	207	34	155	11.2	135	14.4	34.4	4.92	22.2	6.0	2.03	7.2	1.08	6.5	1.30	3.15	0.53	3.25	0.432	4.7
R-Sph-15	1a	313	26	133	9.3	160	14.6	34.2	4.41	22.1	5.3	2.25	6.0	0.88	6.0	1.20	2.86	0.359	2.67	0.392	3.9
R-Sph-17	1a	231	37	178	12.9	162	15.4	38.3	5.3	28.5	7.6	2.13	7.8	1.21	7.2	1.52	3.81	0.54	3.61	0.416	4.3
R-Sph-18	1a	243	37	188	12.9	127	16.6	37.2	5.8	27.6	7.7	2.16	8.4	1.34	8.0	1.53	3.54	0.488	3.29	0.464	4.8
R-Sph-19	1a	248	41	193	13.4	203	19.2	44.0	6.2	29.2	7.8	2.51	8.4	1.30	8.6	1.48	4.31	0.57	3.88	0.55	5.5
R-Sph-20	1a	229	38	181	12.2	156	15.4	36.2	5.3	26.5	7.3	2.06	8.2	1.22	7.5	1.44	4.03	0.50	3.04	0.50	4.9
R-Sph-21	1a	218	36	168	11.5	148	14.5	35.1	4.95	26.0	6.2	1.92	7.2	1.05	7.1	1.34	3.39	0.50	3.17	0.474	4.4
R-Sph-23	1a	238	39	187	12.6	161	16.5	37.8	5.8	24.8	7.3	2.24	7.9	1.28	8.0	1.53	4.09	0.58	3.48	0.52	5.7
R-Sph-24	1a	214	38	178	12.5	138	15.7	36.8	5.6	26.7	6.9	1.99	7.5	1.16	7.1	1.23	3.71	0.54	3.07	0.50	4.5
R-Sph-26	1a	213	34	163	11.4	160	15.2	34.4	4.97	24.4	6.7	1.84	7.3	1.02	7.0	1.38	3.54	0.467	3.08	0.454	4.6
R-Sph-27	1a	219	37	179	12.4	141	15.8	35.6	5.3	23.4	7.2	2.10	7.7	1.15	7.2	1.43	3.62	0.495	3.20	0.413	4.9
R-Sph-30	1a	213	37	175	12.9	145	16.1	39.0	5.5	26.9	7.5	2.14	7.1	1.13	8.0	1.41	3.70	0.490	3.26	0.431	4.9
R-Sph-33	1a	248	37	179	11.6	169	15.7	36.5	5.3	25.1	6.7	2.21	7.4	1.21	7.2	1.56	3.66	0.53	3.48	0.51	5.3
R-Sph-35	1a	208	33	150	11.0	119	13.3	34.2	4.74	22.1	5.4	1.85	6.4	1.00	5.8	1.28	2.96	0.445	2.63	0.383	4.0
R-Sph-5	1b	230	35	182	11.2	179	20.2	42.7	6.3	27.7	7.7	2.09	7.7	1.13	7.2	1.34	3.61	0.480	2.96	0.51	4.8
R-Sph-6	1b	263	35	176	11.7	155	16.9	37.2	5.3	25.7	6.2	2.03	6.8	1.02	6.6	1.19	3.36	0.471	3.03	0.393	4.6
R-Sph-9	1b	242	40	185	12.0	151	17.1	36.1	5.8	25.6	7.1	2.46	8.2	1.32	7.2	1.57	3.89	0.53	3.41	0.472	4.8
R-Sph-12	1b	302	39	198	11.9	193	22.1	46.4	6.6	28.8	7.7	2.35	8.0	1.21	7.4	1.47	3.42	0.489	3.01	0.467	5.3
R-Sph-13	1b	242	32	175	12.6	385	20.0	45.7	5.8	27.2	6.9	2.12	6.5	1.04	6.9	1.18	3.52	0.54	3.38	0.417	5.1
R-Sph-14	1b	247	30	147	10.2	171	17.1	38.9	5.2	22.9	5.5	1.89	6.9	0.89	5.8	1.17	2.78	0.386	2.57	0.419	3.7
R-Sph-22	1b	259	37	180	11.8	186	19.9	42.4	6.1	26.5	7.0	2.14	7.7	1.09	7.6	1.38	3.22	0.465	3.02	0.54	5.0
R-Sph-29	1b	266	37	199	12.1	160	18.5	39.8	6.0	28.7	7.4	2.19	8.5	1.13	7.4	1.24	3.64	0.51	3.31	0.401	5.3
R-Sph-32	1b	263	36	186	12.0	208	18.4	43.0	5.8	26.6	6.4	2.11	8.2	1.19	7.0	1.52	3.31	0.53	3.06	0.288	4.9
R-Sph-34	1b	234	28	149	10.8	152	15.8	36.9	4.94	22.9	5.6	1.81	6.1	0.95	5.7	1.14	2.82	0.414	2.66	0.366	4.4
R-Sph-1	2	267	40	202	14.6	179	17.7	38.8	5.8	29.1	7.3	2.65	8.4	1.28	7.5	1.63	3.63	0.53	3.65	0.52	4.6
R-Sph-10	2	166	45	222	16.8	203	21.3	46.8	6.6	32.2	9.3	2.45	9.5	1.35	8.5	1.89	4.90	0.65	3.90	0.53	6.4
R-Sph-11	2	319	81	374	16.9	175	30.1	36.1	7.5	51	14.8	3.77	17.1	2.42	15.8	3.35	7.8	0.98	7.0	1.03	10.7
R-Sph-16	2	198	40	196	13.8	192	19.1	41.8	5.9	29.7	8.1	2.40	8.7	1.40	8.2	1.64	3.74	0.53	3.29	0.50	5.3
R-Sph-25	2	339	33	231	13.1	306	16.3	26.8	4.86	22.9	5.2	1.86	6.6	0.98	6.5	1.34	3.30	0.480	3.08	0.449	5.4
R-Sph-28	2	197	40	227	16.0	212	20.5	47.4	6.5	30.1	8.9	2.34	8.6	1.27	8.1	1.73	4.06	0.56	3.61	0.493	6.4
R-Sph-31	2	118	51	257	21	250	26.8	58	8.7	39.0	10.1	2.73	11.4	1.54	10.3	2.09	5.2	0.64	4.37	0.65	7.2

Data for chondrites used for normalization are from Taylor and McLennan (1985).

Sample#	Type	Ta (ppm)	Pb (ppm)	Th (ppm)	U (ppm)	W (ppm)	Re (ppm)	Ir (ppm)	Pt (ppm)	Au (ppm)	$La/Sm_{(N)}$	Ni/Cr	Ni/Co	Cr/Co	Fe/Cr
R-Sph-2	1a	0.63	1.57	2.1	0.50	0.330	<LOD	0.032	0.012	<LOD	1.43	3.14	12.15	3.87	292
R-Sph-3	1a	0.62	0.99	2.5	0.54	0.272	<LOD	<LOD	0.0031	<LOD	1.25	4.10	13.24	3.23	351
R-Sph-4	1a	0.63	0.87	2.2	0.44	0.197	<LOD	0.043	<LOD	0.0041	1.35	3.80	12.29	3.24	338
R-Sph-7	1a	0.85	5.0	1.98	0.59	0.414	<LOD	<LOD	0.0024	<LOD	1.40	2.06	3.55	1.72	1288
R-Sph-8	1a	0.70	1.50	2.4	0.44	0.145	<LOD	<LOD	0.011	<LOD	1.51	3.44	7.48	2.17	729
R-Sph-15	1a	0.65	4.6	2.1	0.54	0.186	<LOD	<LOD	0.0042	<LOD	1.74	1.62	5.06	3.13	607
R-Sph-17	1a	0.69	1.85	2.7	0.74	0.488	<LOD	0.009	0.006	<LOD	1.27	2.30	7.50	3.26	467
R-Sph-18	1a	0.71	1.49	2.6	0.54	0.184	<LOD	0.008	<LOD	<LOD	1.37	2.08	4.65	2.24	871
R-Sph-19	1a	0.85	0.51	3.5	0.36	0.180	<LOD	<LOD	0.0009	<LOD	1.54	4.31	11.64	2.70	516

(*continued on next page*)

Table 2 (*continued*)

Sample#	Type	Ta (ppm)	Pb (ppm)	Th (ppm)	U (ppm)	W (ppm)	Re (ppm)	Ir (ppm)	Pt (ppm)	Au (ppm)	$La/Sm_{(N)}$	Ni/Cr	Ni/Co	Cr/Co	Fe/Cr
R-Sph-20	1a	0.70	0.25	2.6	0.31	0.190	<LOD	<LOD	<LOD	<LOD	1.33	4.51	12.21	2.70	407
R-Sph-21	1a	0.73	1.44	2.6	0.62	0.326	<LOD	0.009	0.0010	<LOD	1.48	3.46	13.94	4.03	251
R-Sph-23	1a	0.98	2.1	2.7	0.46	0.275	<LOD	<LOD	0.0047	<LOD	1.42	3.24	11.67	3.61	285
R-Sph-24	1a	0.74	1.49	2.7	0.56	0.249	<LOD	<LOD	0.011	<LOD	1.42	3.39	10.56	3.11	456
R-Sph-26	1a	0.80	1.76	2.4	0.56	0.321	<LOD	<LOD	0.0019	<LOD	1.43	3.86	13.75	3.56	301
R-Sph-27	1a	0.81	2.0	2.7	0.72	0.372	<LOD	<LOD	0.0039	<LOD	1.39	2.76	5.29	1.91	901
R-Sph-30	1a	0.77	0.185	2.9	0.38	0.104	<LOD	<LOD	0.0010	<LOD	1.34	3.03	4.23	1.39	1397
R-Sph-33	1a	0.76	0.58	2.5	0.30	0.188	0.0024	<LOD	0.05	<LOD	1.46	5.97	10.41	1.75	762
R-Sph-35	1a	0.65	2.3	2.2	0.58	0.443	<LOD	<LOD	0.0013	<LOD	1.54	2.71	13.29	4.91	196
R-Sph-5	1b	0.72	4.0	2.9	0.67	0.173	<LOD	<LOD	0.009	0.009	1.65	0.67	1.16	1.72	1235
R-Sph-6	1b	0.70	2.9	2.8	0.62	0.165	<LOD	<LOD	0.012	0.014	1.72	0.64	1.28	2.00	1033
R-Sph-9	1b	0.78	4.1	2.7	0.56	0.158	<LOD	0.017	0.033	0.018	1.51	0.96	1.37	1.43	1591
R-Sph-12	1b	0.65	4.2	3.3	0.65	0.155	<LOD	0.008	0.0015	<LOD	1.81	0.85	1.09	1.28	1878
R-Sph-13	1b	0.85	5.2	3.2	0.81	0.200	<LOD	0.029	0.088	<LOD	1.83	0.64	1.24	1.95	1127
R-Sph-14	1b	0.68	0.95	3.0	0.68	0.096	<LOD	<LOD	<LOD	<LOD	1.94	0.68	1.59	2.33	884
R-Sph-22	1b	0.70	4.1	3.4	0.82	0.305	<LOD	0.018	0.0049	<LOD	1.78	0.57	1.10	1.93	1040
R-Sph-29	1b	0.75	2.9	3.2	0.70	0.216	<LOD	<LOD	<LOD	<LOD	1.58	0.65	1.28	1.97	1057
R-Sph-32	1b	0.57	4.0	2.8	0.55	0.179	<LOD	<LOD	0.0022	<LOD	1.82	0.79	1.12	1.43	1579
R-Sph-34	1b	0.60	3.5	2.5	0.70	0.315	<LOD	<LOD	<LOD	<LOD	1.77	0.56	1.33	2.35	892
R-Sph-1	2	0.93	0.40	3.2	0.28	0.111	<LOD	0.007	0.0019	<LOD	1.52	3.36	7.57	2.25	799
R-Sph-10	2	0.92	1.08	5.3	0.65	0.391	<LOD	0.008	0.011	0.013	1.44	5.19	9.68	1.87	682
R-Sph-11	2	1.67	1.14	6.8	0.61	0.436	0.0042	<LOD	0.0015	<LOD	1.28	3.99	13.51	3.39	371
R-Sph-16	2	0.84	0.047	4.0	0.130	0.102	<LOD	<LOD	0.006	<LOD	1.48	4.45	6.14	1.38	1003
R-Sph-25	2	1.08	11.1	4.2	0.51	0.248	0.0036	<LOD	<LOD	<LOD	1.96	1.03	4.95	4.79	590
R-Sph-28	2	1.05	0.71	4.5	0.48	0.361	<LOD	<LOD	0.028	<LOD	1.45	3.96	6.55	1.66	962
R-Sph-31	2	1.31	6.0	7.2	1.22	0.93	<LOD	0.008	<LOD	<LOD	1.67	3.09	6.34	2.06	759

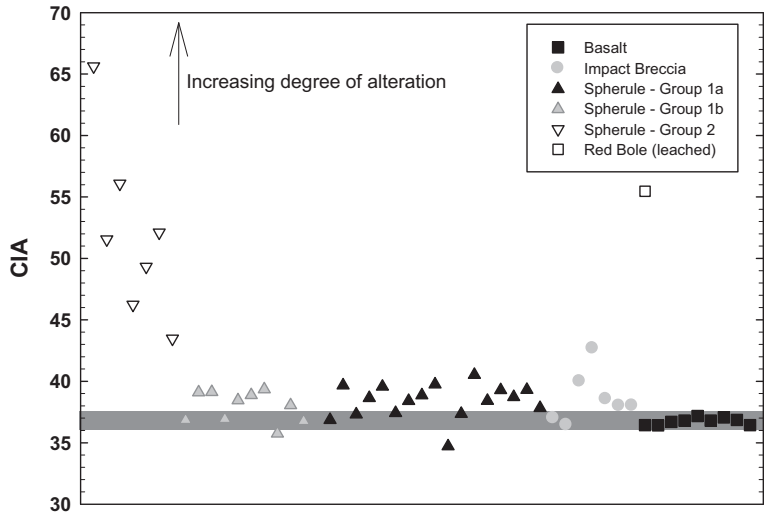

Fig. 2. Chemical index of alteration (CIA) values of the basalts, red bole (leached), impact breccia and spherules from the Lonar crater. The shaded bar reflects the 2SD of the average CIA of the basalts. The impact breccia samples and most spherules (Group 1) show overlapping and slightly higher CIA values than the basalts. Seven spherules show significantly higher CIA values and are classified as Group 2. Group 1 spherules are further divided into types 1a and 1b based on additional criteria, particularly the high Ni concentration in Group 1a spherules. See text for details.

spherules showing the lowest values (Fig. 3a and b). Some of the impact breccia and Group 1b spherules exhibit elevated EF_K (>1) (Fig. 3a). Group 1a spherules are characterized by the highest values for EF_{Ni} and EF_{Cr}, followed by the Group 2 spherules (Fig. 3c), while the Group 2 and Group 1b spherules show relatively high EF_{Th} (Fig. 3d). The spherules show large variations in both EF_{Cu} and EF_{Zn} compared to the melt rocks and impact breccia, which show slight depletions in both EF_{Cu} and EF_{Zn} (Fig. 3e). The EF_{Zn} in the spherules, particularly Group 1a, show a positive correlation with EF_{Pb} (Fig. 3f), EF_K (Fig. 3g) as well as EF_{Na} (Fig. 3h). Barring the high EF_K, EF_{Ca} and EF_{Pb}, the composition of the bulk red bole overlaps with that of the basalts and impact breccia (Fig. 3).

3.3. Moderate and highly siderophile elements

Cobalt concentrations in the basalts (118–131 ppm) and impact breccia (111–130 ppm) show a limited and overlapping range. In contrast, Ni and Cr concentrations in the basalts and impact breccia show larger ranges. Barring the basalts R1 and L10 with 109 ppm and 112 ppm Cr, respectively, the basalts range from 34 to 62 ppm in Cr, whereas the impact breccia range from 65 to 102 ppm in Cr. The basalt samples R1 and L10 also show higher Ni concentrations (79 and 86 ppm, respectively) compared to the other basalts (52–55 ppm). Most impact breccia samples show overlapping Ni concentrations (52–136 ppm) with the basalts. The bulk red bole sample shows distinctly lower Co (68 ppm) but overlapping Cr (47 ppm) and Ni (54 ppm) concentrations compared to the basalts.

Concentrations of Cr, Ni and Co in the spherules show relatively large ranges (Table 2). Cobalt concentrations in the Group 1 spherules (46–140 ppm) overlap, but those of Group 2 spherules (43–103 ppm) show distinctly lower values than those of the basalts and impact breccia (111–131 ppm). The Group 1 spherules are further sub-divided into Group 1a (n = 18), which exhibit high Ni concentrations (205–1855 ppm) and Group 1b (n = 10) showing lower Ni concentrations (48–75 ppm). In addition, Group 1a spherules broadly show higher Co and Cr concentrations as well as significantly higher Ni/Cr (>1) and Ni/Co (>2) than Group 1b spherules (Table 2 and Fig. 7a, b). The spherules show higher Cr/Co compared to the basalts and impact breccia, while Fe/Cr of the spherules and impact breccia overlap and are distinctly lower than that of the basalts (Table 2 and Fig. 7a).

Concentrations of the highly siderophile elements (HSE) Re, Ir, Pt, Au are reported for the first time for selected spherules from the Lonar crater (Table 2). For several spherules, the concentrations of the HSE were below the procedural limits of detection (LOD, Supplementary Table A.1). While concentration data are limited to 3 and 5 spherules for Re and Au, respectively, Ir abundances are reported for 12 spherules (5 in Group 1a, 4 in Group 1b and 3 in Group 2), while Pt concentrations are reported for 26 spherules (15 in Group 1a, 7 in Group 1b and 5 in Group 2; Table 2). Iridium concentrations in the different spherule groups show overlapping values ranging from 7 to 43 ppb, with the Group 1a spherules showing the highest measured Ir concentrations at Lonar (Fig. 4). Platinum concentrations range from 0.9 to 88 ppb. Four spherules (R-Sph-9, 13, 28, 33) show significantly high concentrations (>28 ppb) compared to the other spherules (Table 2).

3.4. Non-siderophile elements

The basalt samples, with the exception of R1 and L10, show limited variability in non-siderophile element concentrations. Compared to the other basalts, samples R1 and

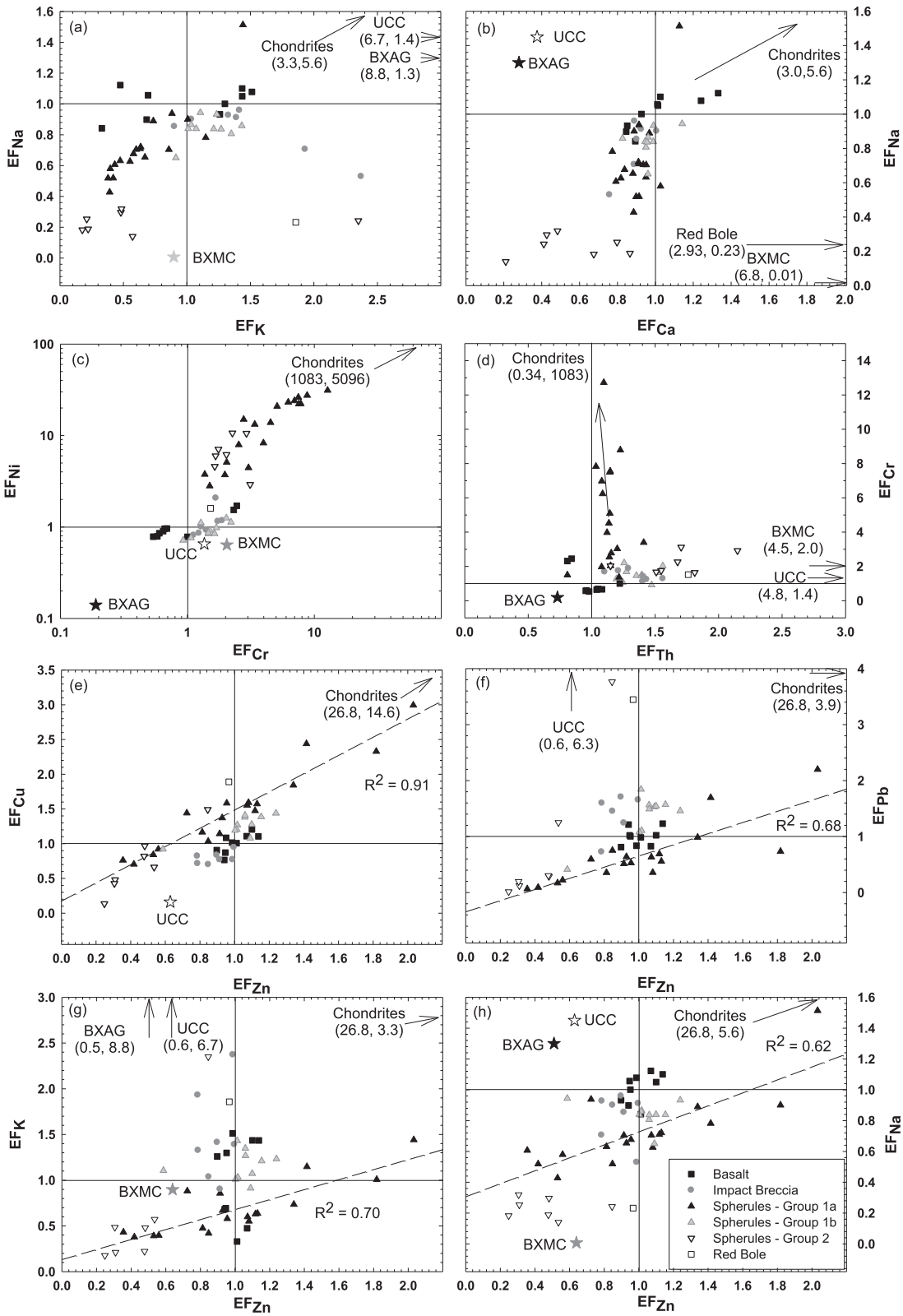

Fig. 3. Co-variation of enrichment factors (EF) of (a) Na-K, (b) Na-Ca, (c) Ni-Cr, (d) Cr-Th, (e) Cu-Zn, (f) Pb-Zn, (g) K-Zn and (h) Na-Zn in individual basalts, impact breccia, spherules and the bulk red bole sample. The value of 1, shown by the horizontal and vertical lines, denotes the composition of the average basalt. Also shown for comparison are the EF values of the above-mentioned elements for average chondrites (data from Mason (1979) and Tagle and Berlin (2008)), upper continental crust (UCC) (McLennan, 2001) as well as basement xenoliths in Deccan basalts (Ray et al., 2008) including an augen gneiss (BXAG) and a meta-carbonate (BXMC). The variations in EF of the different elements are explained in terms of aqueous alteration, contribution from a chondritic impactor, basement melting, as well as evaporation-condensation effects. See text for details.

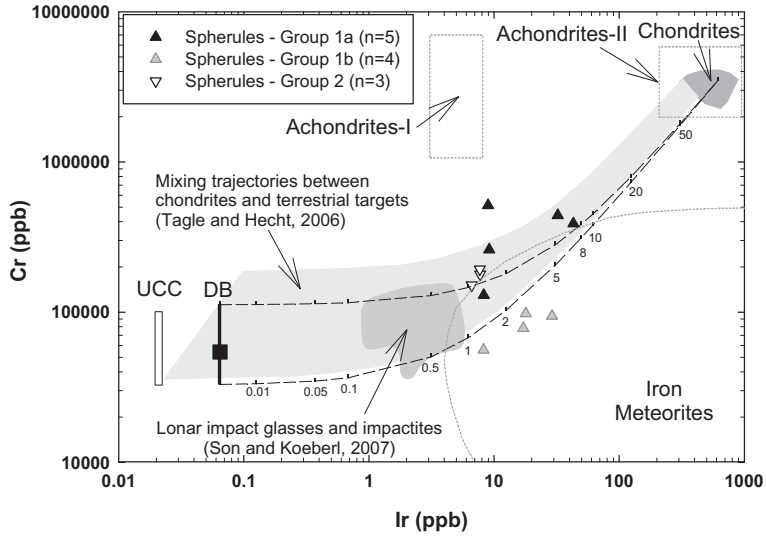

Fig. 4. A plot of Cr versus Ir concentrations in selected Lonar spherules. Also shown for comparison are the average composition (filled square) and compositional ranges (filled vertical bar) of basalts at Lonar (Ir data from Crocket and Paul, 2004; Cr data from the present study), UCC (data from Taylor and McLennan, 1985; Peucker-Ehrenbrink and Jahn, 2001; McLennan, 2001; Rudnick and Gao, 2003), average chondrites (Tagle and Berlin, 2008), iron meteorites, PGE-rich (labelled type II) and PGE-poor (labelled type-I) achondrites (Tagle and Hecht, 2006) as well as data for Lonar impact glasses and impactites (Son and Koeberl, 2007). The light gray band represents the likely mixing trajectories between chondritic impactors and common terrestrial target rocks (Tagle and Hecht, 2006). The Lonar spherules fall on a mixing trend between average chondrites and the average Deccan basalts with 1–8 wt% contribution from a chondritic impactor. See text for details.

L10 show slightly higher Al and Ca but lower concentrations of Na, Ti as well as of most trace elements, including REE (Table 1). Concentrations of most non-siderophile elements in the impact breccia broadly overlap with those of the basalts barring K, Rb, Th, Pb, and Ba, the concentration of which are higher in many of the impact breccia samples relative to the basalts (Table 1). The bulk red bole sample shows depletion in Na but significant enrichments in K and Ca compared to the target basalt (Table 1). Group 1a spherules broadly show higher MgO concentrations than Group 1b spherules, while Group 1b spherules show slightly higher SiO_2 and Al_2O_3 abundances (Table 2). Major element compositions of the Group 2 spherules overlap with both Group 1a and 1b spherules (Table 2).

On chondrite-normalized REE concentration plots (chondrite values from Taylor and McLennan, 1985), the basalts and impact breccia are generally characterized by light REE (LREE) enriched patterns (Fig. 5a), similar to what has been observed in an earlier study (Chakrabarti and Basu, 2006). However, the impact breccia samples show higher LREE fractionation ($La/Sm_{(N)} = 1.52–1.88$) compared to the basalts ($La/Sm_{(N)} = 1.27–1.57$) (Table 1). The LREE fractionation observed for the Group 1a spherules ($La/Sm_{(N)} = 1.25–1.54$; value for R-Sph-15 is 1.74) is mostly lower than that for Group 1b ($La/Sm_{(N)} = 1.51–1.94$) (Table 2; Figs. 5a and 7c). The extent of LREE fractionation for the Group 1a spherules is similar to that of the basalts while the Group 1b spherules show higher LREE fractionation broadly similar to that of the impact breccia (Tables 1 and 2; Figs. 5a and 7c). Group 2 spherules show a wider range in $La/Sm_{(N)}$ values (1.28–1.96) and overlap with the $La/Sm_{(N)}$ values of both Group 1a and Group 1b spherules (Table 2; Figs. 5a, and 7c). Compared to the basalts as well as the impact breccia and spherules, the red bole sample exhibits significantly lower REE concentrations (Table 1 and Fig. 5a). In primitive mantle-normalized trace element concentration patterns (primitive mantle values from Sun and McDonough, 1989), the impact breccia show higher concentrations of the LILE compared to the basalts (Fig. 5b). The Group 1b and some of the Group 2 spherules show higher concentrations of LILE (Fig. 5b) compared to the Group 1a spherules. Most of the Group 1a and Group 2 spherules show prominent depletions in Pb, which are significantly larger than those of the target basalts (Fig. 5b). In contrast, most of the Group 1b spherules (barring R-Sph-14) do not show any negative Pb anomaly (Fig. 5b). The Group 1b spherules also show negative Nb and Ta anomalies, similar to the impact breccia, which are not observed for the other spherules (Fig. 5b). The red bole sample shows positive Pb and Zr anomalies, relatively high Rb, Th and U concentrations, and a distinct negative Ba anomaly and this pattern is not observed in any other sample from Lonar (Fig. 5b).

3.5. Neodymium and strontium isotope ratios

Neodymium and Sr isotopic compositions for selected basalts, impact breccia, non-spherical impact glasses (14 combined together) and the red bole sample are reported in Table 3 and shown in Fig. 6a. For the spherule samples labelled as "Spherules-large" (average diameter of ~500 μm) and "Spherules-small" (average diameter of ~250 μm), only Sr isotopic data are reported (Table 3 and Fig. 6a, b). These spherules were not analyzed for their

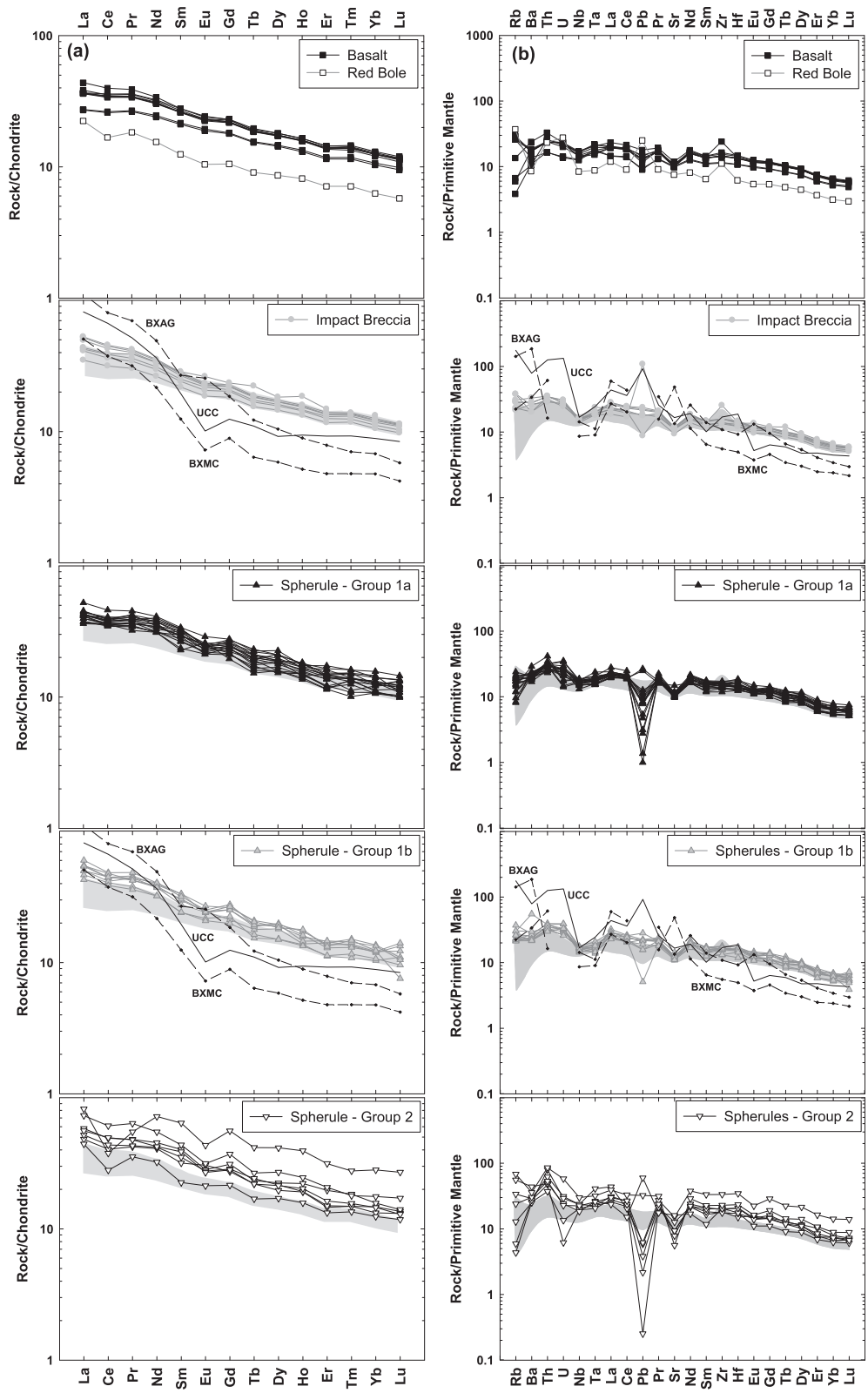

Fig. 5. (a) Chondrite (CI)-normalized REE patterns and (b) Primitive mantle-normalized abundances of trace elements arranged in order of increasing compatibility towards the right for the Lonar basalts, red bole, impact breccia and spherules. REE concentration data for chondrites are taken from Taylor and McLennan (1985) and primitive mantle trace element concentration data are taken from Sun and McDonough (1989). Also plotted for comparison are data for the average UCC (McLennan, 2001) as well as for augen gneiss (BXAG) and meta-carbonate (BXMC) basement xenoliths in the Deccan basalts (Ray et al., 2008). The gray shades denote the composition of the basalts at Lonar. See text for details.

Table 3
Neodymium and strontium isotope composition of selected target basalts, impact breccia, large and small spherules, non-spherical impact glasses, and red bole from the Lonar crater.

Sample#	Rock type	Nd (ppm)	Sm (ppm)	Sm/Nd	$^{143}Nd/^{144}Nd_{(0)}$	$\varepsilon_{Nd_{(0)}}$	Rb (ppm)	Sr (ppm)	Rb/Sr	$^{87}Sr/^{86}Sr_{(0)}$
R1	Basalt	17.0	4.87	0.29	0.512778	2.73	16.4	207	0.079	0.706128
R3	Basalt	22.6	6.2	0.27	0.512702	1.25	18.8	213	0.088	0.706639
R4	Basalt	24.2	6.4	0.27	0.512562	−1.48	8.6	251	0.034	0.707235
R5	Basalt	23.1	6.4	0.28	0.512675	0.72	4.2	225	0.019	0.706288
R6	Basalt	21.7	6.0	0.28	0.512711	1.42	16.6	216	0.077	0.706329
R7	Basalt	22.1	6.0	0.27	0.512692	1.05	3.8	230	0.017	0.706410
RLL1	Basalt	21.8	6.1	0.28	0.512708	1.37	16.8	219	0.077	0.706751
L10	Basalt	17.5	4.98	0.28	0.512777	2.71	2.4	214	0.011	0.705639
R5b	Impact breccia	24.8	6.4	0.26	0.512369	−5.25	18.5	248	0.074	0.708025
R6b	Impact breccia	25.3	6.5	0.26	0.512368	−5.27	19.5	252	0.078	0.708639
R7b	Impact breccia	24.0	6.2	0.26	0.512379	−5.05	17.9	247	0.072	0.708105
L8	Impact breccia	22.2	5.8	0.26	0.512518	−2.34	24	236	0.101	0.708091
L27A	Impact breccia	18.8	5.0	0.27	0.512608	−0.59	24	198	0.122	0.707707
R9	Impact breccia	21.2	5.6	0.26	0.512498	−2.73	14.8	233	0.063	0.707900
R7s-ig	Non-spherical impact glass				0.512244	−7.69				0.707834
R7s-sl	Spherules-large									0.707234
R7s-ss	Spherules-small									0.707589
RRB	Red Bole (bulk)	11.0	2.88	0.26	0.512534	−2.03	24	160	0.148	0.707520

Rb/Sr and Sm/Nd ratios are calculated from the ICPMS trace element concentration data in Table 1. $\varepsilon_{Nd_{(0)}}$ is calculated using the present-day bulk earth (CHUR) value of $^{143}Nd/^{144}Nd = 0.512638$. The $\varepsilon_{Nd_{(0)}}$ values represent the deviation of $^{143}Nd/^{144}Nd$ in parts per 10^4 from the present-day CHUR value.

elemental concentrations and are hence not classified into different groups. The Nd isotopic measurements of these spherules were not successful because of the limited amount of sample processed. The impact breccia samples show less radiogenic $^{143}Nd/^{144}Nd$ ratios ($\varepsilon_{Nd(0)} = -0.59$ to -5.27) than the target basalts ($\varepsilon_{Nd(0)} = -1.48$–$2.73$), and more radiogenic $^{87}Sr/^{86}Sr$ ratios (0.707707–0.708639) compared to the basalts (0.705639–0.707235) (Table 3). A re-analyzed basalt (L10) and impact breccia (L27A) sample from the earlier study of Chakrabarti and Basu (2006) yielded consistent results. The non-spherical impact glasses ($\varepsilon_{Nd(0)} = -7.69$; $^{87}Sr/^{86}Sr = 0.707834$) exhibit the most unradiogenic Nd isotopic composition of all rock samples from Lonar analyzed until today (Fig. 6a). The Nd isotopic composition of the red bole ($\varepsilon_{Nd(0)} = -2.03$) overlaps with that of the basalts at Lonar, but this sample shows slightly more radiogenic Sr ($^{87}Sr/^{86}Sr = 0.707520$) compared to the basalts (Fig. 6a).

3.6. Volatile elements

Concentrations of the relatively fluid immobile volatile elements Cu and Zn show a wide range in the Group 1a and Group 2 spherules (Cu = 111–412 ppm, Zn = 48–173 ppm), compared to the more restricted ranges observed for the Group 1b spherules (Cu = 32–108 ppm, Zn = 3.8–43 ppm) as well as the basalts, red bole and impact breccia (Cu = 96–160 ppm, Zn = 84–108 ppm) (Tables 1 and 2). While the Group 1a spherules show significant enrichments in Zn and large enrichments in Cu, most of the Group 2 spherules show depletions in Zn and Cu relative to the basalts. The Group 1b spherules show slightly higher Zn and distinctly higher Cu concentrations compared to the basalts and impact breccia (Fig. 8). The Group 1a and Group 2 spherules also show large variations in EF_{Cu} and EF_{Zn} and these variations show a rough positive correlation (Fig. 3e). For the Group 1a spherules, EF_{Zn} is also correlated with EF_{Pb}, EF_K and EF_{Na} (Fig. 3f, g, h).

4. DISCUSSION

4.1. Screening for alteration of the impactites at Lonar

The occurrence of a saline lake in the Lonar crater, the overall high amount of rainfall received in this region, and the susceptibility of basaltic rocks to aqueous alteration (e.g., Gaillardet et al., 1999) suggest that chemical weathering of the Lonar impactites and target basalts could have played a significant role in modifying the geochemical composition of the samples since its formation ~ 570 ka ago (Jourdan et al., 2011). To quantify the extent of chemical alteration, the CIA values of the basalts, impact breccia and spherules were calculated (Tables 1 and 2). This approach is particularly useful to distinguish variations in concentrations of elements that are affected by both aqueous alteration as well as impact processes. For example, elements like Na, K and Rb are both fluid mobile as well as volatile, and variations in the concentrations of these elements in impactites need to be assessed by screening the samples for aqueous alteration. The low CIA values of the basalts and impact breccia samples suggest minimal effects of aqueous alteration in these samples. Hence, their geochemical and isotopic variability can be interpreted in terms of compositional heterogeneity of the Deccan basalt or impact related processes. The CIA value of the bulk red bole sample, formed within the flows of the Deccan

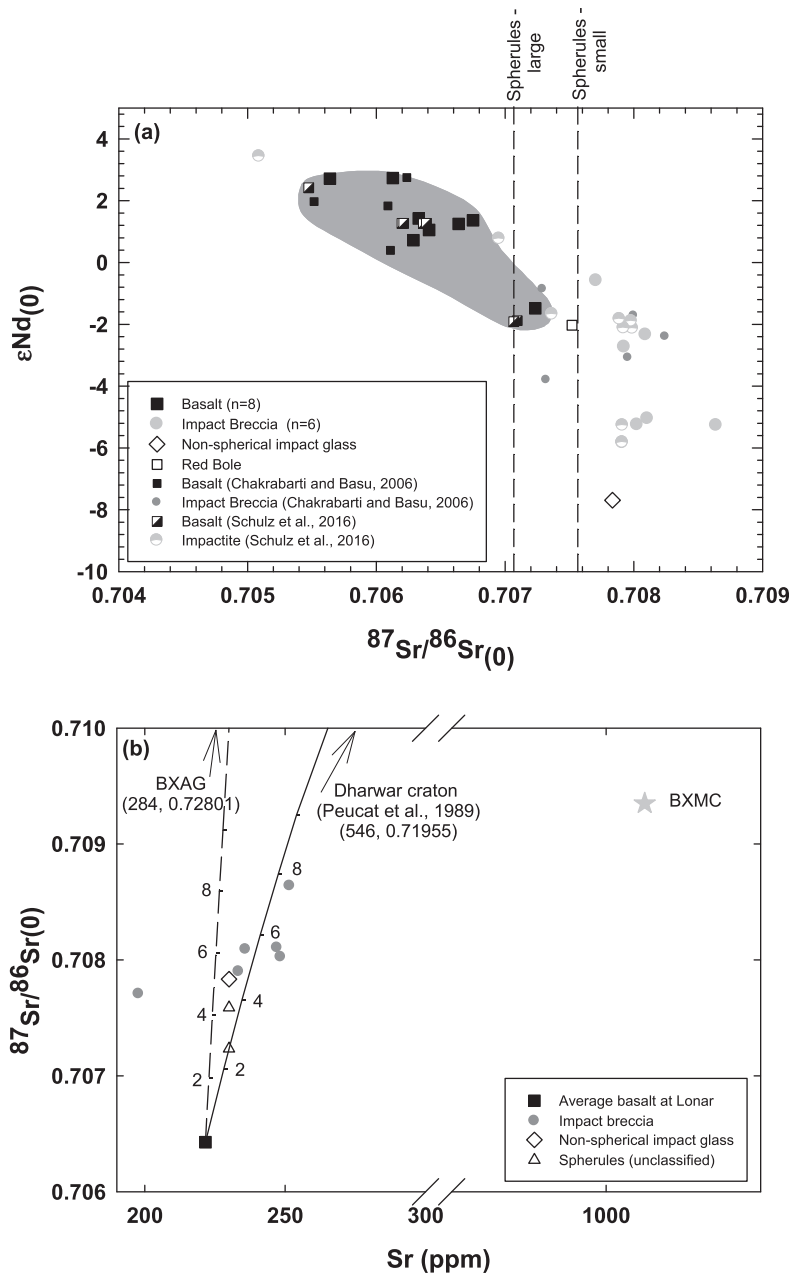

Fig. 6. (a) Measured Nd and Sr isotopic compositions of the Lonar basalts, red bole, impact breccia and non-spherical impact glasses. The two vertical lines indicate the Sr isotopic compositions of combinations of large (~500 μm diameter) and small (~250 μm diameter) spherules. The compositions of the Lonar basalt, impact breccia and impactites from previous studies (filled gray symbols, Chakrabarti and Basu, 2006; Schulz et al., 2016) are also plotted for comparison. (b) A plot of Sr isotopic composition versus Sr concentration of the Lonar impact breccia, non-spherical impact glasses, 'large' and 'small' spherules and the average target basalt at Lonar. Also shown for comparison are the compositions of a meta-carbonate basement xenolith (BXMC), an augen gneiss basement xenolith (BXAG) (Ray et al., 2008) and Dharwar craton granitoids (Peucat et al., 1989). Mixing calculations suggest 2–8 wt% contribution of the basement to the Lonar impactites. Higher contributions of the basement, up to ~15 wt%, are based on Nd isotopic constraints. See text for details.

Traps, is anomalously low (20.4). This low value is due to the high Ca concentration in the sample (11.7 wt%, Table 1), which is most likely contributed by recent soil carbonates. Hence, the red bole was leached with 2% acetic acid to selectively dissolve the carbonates, after which the CIA value of the silicate residue was determined to be 55.6 (Table 1). The high CIA of the leached red bole, compared to the unaltered basalts (Fig. 2), is consistent with its origin by aqueous alteration of the Deccan basalts (Wilkins et al., 1994).

The CIA values of the spherules were determined to understand the degree of alteration of these sub-mm-sized impact glasses. The spherules were initially screened by examining the surface textures (e.g., "pitted" versus

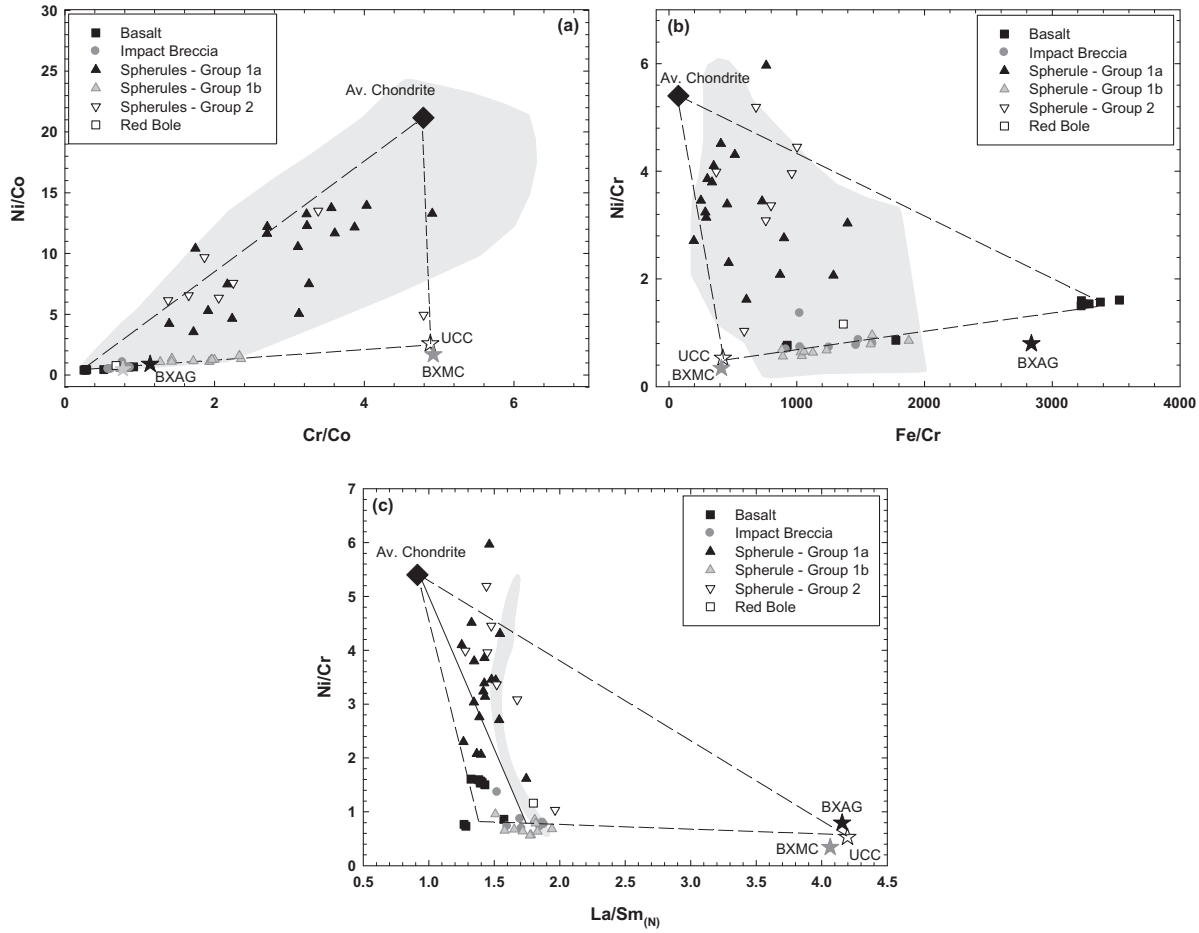

Fig. 7. Plots of (a) Ni/Co versus Cr/Co, (b) Ni/Cr versus Fe/Cr, and (c) Ni/Cr versus $La/Sm_{(N)}$ showing compositions of the Lonar basalts, impact breccia, spherules as well as the bulk red bole. Also shown for comparison are the compositions of the Lonar spherules from Misra et al. (2009) and Ray et al. (2017) (gray shade). The compositions of the Lonar spherules can be explained by mixing between three components - target basalts, a chondritic impactor, and the basement underlying the Deccan basalts. The impact breccia and Group 1b spherules plot on a mixing line between the basalts and the basement represented by the UCC, BXMC and BXAG (Fig. 7c only), whereas most of the Group 1a and Group 2 spherules show dominant contribution from a chondritic impactor.

"smooth"), first using a binocular stereomicroscope, followed by evaluation of BSE images (Fig. 1c). However, no apparent relationship was observed between the CIA values of the spherules and the extent of surface alteration as inferred by visual inspection of the BSE images. Some of the Group 1 spherules show pitted surfaces but are geochemically least altered, while some of the Group 2 spherules, which show geochemical evidence for significant alteration, do not show any signs of surface alteration. The lack of any apparent relationship is due to the non-uniform extent of alteration and the small area of sampling/ablation (~50 μm in diameter, few 10s of μm in depth) of the spherule during LA-ICPMS measurements. For example, aqueous alteration in a spherule with a high number of surface pits may not always be pervasive. Even for such a spherule, a relatively smooth surface was chosen for LA-ICPMS measurements and the sampling point need not always be affected by alteration. On the contrary, a spherule with lesser number of surface pits may have experienced pervasive aqueous alteration leading to loss of fluid mobile elements. Analyses of such a spherule using LA-ICPMS, again on a smooth surface spot, will exhibit loss of these elements and a high CIA value. Hence, the use of CIA values to screen spherules for aqueous alteration represents a more quantitative approach.

4.2. Geochemical variability of the impactites compared to the target basalts at Lonar

Elemental concentration variations in the different types of impactites at Lonar compared to the target basalts can be caused by a variety of processes. In addition to post-impact aqueous alteration, impact related processes, such as melting, mixing and volatilization/condensation, may cause enrichments or depletions in the concentrations of different elements. To evaluate the relative roles of the above-mentioned processes as well as preferential melting of minerals in the target rocks upon impact and the role of K-rich hydrothermal fluids, enrichment factors (EF) for different elements were calculated (Fig. 3). Using pub-

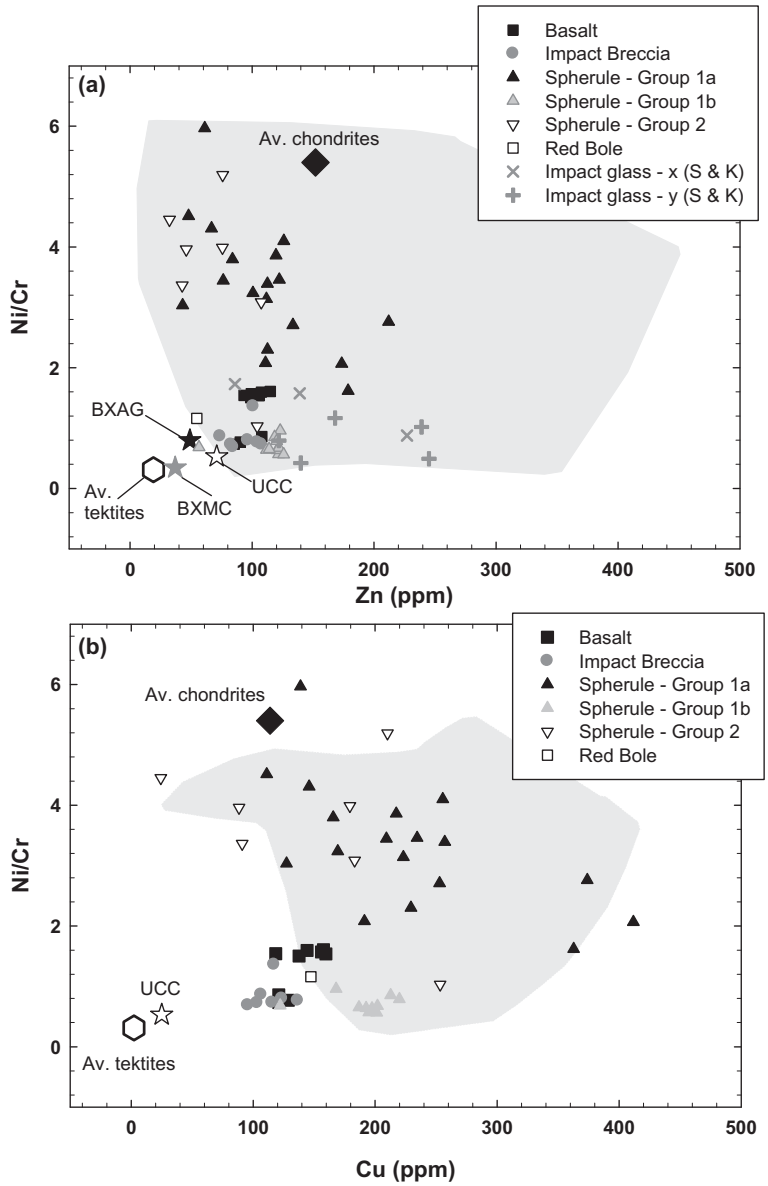

Fig. 8. Plots of (a) Ni/Cr versus Zn and (b) Ni/Cr versus Cu showing compositions of the Lonar basalts, impact breccia, spherules as well as the bulk red bole. The impact breccia, basalts as well as the Group 1b spherules show restricted Ni/Cr as well as Cu and Zn concentrations, while the Group 1a and Group 2 spherules show a larger range of values. Our spherule data overlap with published data for Lonar spherules (gray shade) (Misra et al., 2009; Ray et al., 2017) but show higher Zn and Cu concentrations as well as Ni/Cr than different tektites from all major tektite strewn fields (labelled as Av. tektites, Moynier et al., 2009, 2010). Also shown for comparison are Zn concentrations for Lonar impact glasses (Son and Koeberl, 2007). These impact glasses have been labelled x and y based on their Zn isotopic composition (Moynier et al., 2008). See text for details.

lished data, EF for average chondrites, the Upper Continental Crust (UCC), and Deccan basement rocks were also assessed (Fig. 3). For chondrites, elemental concentrations used for this study are from Mason (1979), except for Cr, Ni and Co, which were compiled in Tagle and Berlin (2008). Data for the geochemical composition of the average UCC are from McLennan (2001). The compositions of representative samples of the heterogeneous basement underlying the Deccan basalts are taken from Ray et al. (2008). These basement rocks include an augen gneiss, the composition of which is considered to be similar to that of the average Archean felsic crust (Ray et al., 2008), and a meta-carbonate, both of which were found as xenoliths within the Deccan basalts. The augen gneiss is referred to as BXAG and the meta-carbonate as BXMC (Figs. 3 and 5–8).

We first consider the EF values of the elements which can be affected by evaporation/condensation effects as well as fluid alteration. Sodium and K are volatile elements (50% T_C of 958 K and 1006 K, respectively), while Ca is

refractory (50% T_C of 1517 K) (Lodders, 2003). These elements are also fluid mobile. The high CIA values in the Group 2 spherules, suggesting aqueous alteration of these samples, could also be explained by preferential depletions of K and Na due to impact volatilization (Fig. 3a) relative to Ca (see Eq. (1)). However, the Group 2 spherules also show lower EF_{Ca} compared to the basalts suggesting loss of Ca (Fig. 3b). Hence, the high CIA values for the Group 2 spherules are considered to reflect fluid alteration processes rather than volatilization during impact.

Unlike the Group 2 spherules, Group 1a and 1b spherules both show basalt-like EF_{Ca} (Fig. 3b) and low CIA values (Fig. 2), the latter suggesting a relatively unaltered nature of these spherules. However, EF_{Na} in the Group 1a spherules is lower than in Group 1b spherules, which in turn overlaps with the basalts (Fig. 3a). This difference in EF_{Na} between Groups 1a and 1b and the depletion in Na in Group 1a relative to the basalts cannot be explained by different extents of aqueous alteration, given the overlapping CIA values of the Group 1a and 1b spherules, and thus requires an additional explanation. One possible explanation is impact-induced volatile loss of Na in the Group 1a spherules, discussed further in Section 4.5.

Preferential melting of plagioclase in the target basalt upon impact has been suggested as a possible mechanism to explain the enrichment of LILE in the impact melts (Misra and Newsom, 2011; Ray et al., 2017) and this process could also affect the CIA values of the impactites. Sodium and Ca are the dominant elements in plagioclase. However, with the exception of three samples, none of the spherules and melts from Lonar show any enrichment in Na and Ca relative to the basalts (EF_{Na}, EF_{Ca} less than 1, Fig. 3b). Hence, any significant role of plagioclase melting in affecting the CIA values or EF values of the impactites can be ruled out.

Like the EF_{Na}, the EF_K in the Group 1a spherules is also lower than in the Group 1b spherules (Fig. 3a), which could reflect loss during impact volatilization (cf., discussion in Section 4.5). However, unlike the EF_{Na}, the EF_K values of the Groups 1a and 1b spherules both overlap with those of the individual basalt samples. Alternatively, the large variability in K concentrations in the basalts and the high EF_K observed in the Group 1b spherules could also reflect the involvement of a hydrothermal fluid (cf., Hagerty and Newsom, 2003; Ray et al., 2017). However, the Group 1b spherules with K excesses also have higher SiO_2 concentrations (>50 wt.%) (Table 2), which is not likely to be derived from a K-rich hydrothermal fluid (Hecht et al., 2004). Overall, the variability in EF_{Ca}, EF_{Na} and EF_K values of the Lonar spherules rule out preferential melting of plagioclase in the target basalt upon impact and hydrothermal alteration, but rather reflect aqueous alteration (Group 2 spherules) and/or impact-related volatilization (Group 1a spherules).

4.3. No contribution of the red bole to the compositions of the Lonar impactites

The red bole sample from Lonar analyzed in this study is representative of the wide-spread clay-rich horizons formed in between different flows of the Deccan Traps. The occurrence of red boles within flows of the Deccan Traps is indicative of their contemporaneous formation ~65 Ma ago with the eruption of the Deccan Traps (Wilkins et al., 1994). Excluding Ca and to some extent K, the concentrations of most major elements in the red bole are mostly lower relative to the Lonar basalts and impactites (Table 1). Trace element concentrations of the red bole are also typically lower, with the exception of the elevated concentrations for Rb and Pb (Tables 1 and 2). Although the EF values of Na, Cr, Th and Zn (Fig. 3) as well as $La/Sm_{(N)}$ values (Fig. 7c) of the red bole overlap with some of the Lonar impactites, the concentrations of these elements are lower in the red bole compared to the majority of the impactite samples (Tables 1 and 2). The lower element concentrations in the red bole relative to the impactites rule out the possibility of the impactite compositions being affected by incorporation of the red bole material during impact. The Nd and Sr isotopic compositions of the red bole plots between the target basalts and the impact breccia (Fig. 6a). Hence, it could not have contributed to the typically more radiogenic Sr and less radiogenic Nd isotopic composition of the impact breccia. Overall, the lower trace element concentrations as well as the Nd and Sr isotopic compositions of the red bole sample rule out significant contributions of this lithology to the composition of the impactites at Lonar.

4.4. Nature of the impactor at Lonar and its relative contribution to the spherules

Concentrations of the HSE (e.g., Ir and Pt) as well as the MSE (e.g., Ni, Cr, Co) are powerful tracers of meteoritic inputs in impactites because their concentrations are much higher in most meteorites (e.g., chondrites, irons, primitive achondrites) than in terrestrial rocks. These elements, along with Fe, are relatively immobile in most conditions and, more importantly, exhibit elemental ratios that allow the identification of the type of impactor even after its mixing with complex/layered targets (Palme et al., 1978; Evans et al., 1993; Koeberl, 1998; Tagle and Hecht, 2006; Tagle and Berlin, 2008; Koeberl et al., 2012; Goderis et al., 2013). Compared to felsic target rocks, extracting the geochemical and isotopic signature of an impactor on basaltic target rocks, like at Lonar, poses additional challenges because basalts have higher concentrations of MSE and HSE compared to felsic rocks (cf., Schulz et al., 2016).

Compared to the MSE, HSE concentrations are more sensitive to meteoritic inputs because of their lower concentrations in terrestrial, particularly mafic, target rocks (Koeberl, 1998, 2002; Goderis et al., 2012). However, Pt concentrations in the spherules do not allow detection of the impactor at Lonar because of the relatively high concentration of Pt in terrestrial basalts compared to Ir (Rehkamper et al., 1999; Schulz et al., 2016). Some of the Lonar spherules contain Ir concentrations of 7–43 ppb (Table 2), significantly elevated compared to the average UCC (~0.02 ppb) (cf., McLennan, 2001; Peucker-Ehrenbrink and Jahn, 2001; Rudnick and Gao, 2003) or the Deccan basalts (average 0.067 ppb) (Crocket and Paul, 2004; Schulz et al., 2016), suggesting contributions

from a meteoritic component. The Ir concentrations in the spherules show a relatively constricted range, possibly because the sub-ppb values could not be detected as a result of the LOD of 1 ppb Ir for the applied method. On a plot of Cr versus Ir concentrations (Fig. 4), the Lonar spherules plot on a mixing trend between average Deccan basalts (Ir data from Crocket and Paul, 2004, Cr data from the present study) and average chondrites (data from Tagle and Berlin, 2008) and broadly overlap with the mixing trajectories between chondritic impactor and common types of terrestrial rocks (Tagle and Hecht, 2006). These observations suggest that the impactor at Lonar was a chondrite.

In the same discrimination diagram (Fig. 4), the field of iron meteorites plots to the bottom right and overlap with the composition of some of the Lonar spherules. However, most Group 1a spherules show higher Cr compared to iron meteorites (Fig. 4) as well as higher Cr/Co (Table 2) compared to average iron meteorites (<0.06) (Goderis et al., 2013). The Fe/Cr ratios in the Lonar spherules are lower than the target basalts (Fig. 7b), while iron meteorites are expected to mostly have higher Fe/Cr of 2000–60,000 (data from Mason, 1979; Goderis et al., 2013). In addition, Ni/Cr ratios in iron meteorites range from 379 to 4000 (Goderis et al., 2013 and references therein). In the Ni/Cr versus Fe/Cr discrimination diagram (Fig. 7b), a three component mixing between iron meteorites (not plotted), basalts and basement rocks cannot explain the compositions of the Lonar spherules. Based on the above arguments, we rule out an iron meteorite impactor at Lonar.

Certain types of achondrites like HEDs and angrites (labelled as type I in Fig. 4) have lower Ir concentrations (<10 ppb) than the Lonar spherules (7–43 ppb) and hence, could not have been the impactor at Lonar. High HSE-bearing achondrites like brachinites, ureilites, lodranites, acapulcoites and winonaites (primitive achondrites, labelled as type II in Fig. 4) exhibit Cr and Ir concentrations partly overlapping with chondrites (Fig. 4). However, most of these type II achondrites show Ni/Co and Cr/Co values (Kallemeyn and Wasson, 1985; Goderis et al., 2013 and references therein) that overlap with or are lower than those of the Lonar spherules (Fig. 7a) and hence, could not have been the impactor at Lonar.

Simultaneous measurements of the concentrations of Cr and Ir (upper limits of concentration) in impact glasses and impactites from Lonar have previously been reported (Son and Koeberl, 2007). The concentrations of Ir in these samples are lower (upper estimates ranging from 1.8 to 3.3 ppb) than those observed in the spherules reported in this study (7–43 ppb). However, on the Cr versus Ir plot (Fig. 4), the Lonar impact glasses and impactites from Son and Koeberl (2007), measured using instrumental neutron activation analysis (INAA), also plot on the same mixing trend between average target basalts at Lonar and chondrites, consistent with a chondritic impactor at Lonar. Using MSE (Ni, Cr, Co) concentrations and ratios in spherules, Misra et al. (2009) also argued for a chondritic impactor at Lonar. Using the same geochemical proxies, a more recent study (Ray et al., 2017) has argued for an EH-type chondrite impactor, whereas based on Cr isotopic measurements of impactites, a carbonaceous chondrite impactor has been suggested for the Lonar impact crater (Koeberl et al., 2017).

Mixing calculations between average Deccan basalts and average chondrites suggest that the Lonar spherules contain a chondritic contribution equivalent to 1–8 wt% (Fig. 4). Our estimate is lower than that of Misra et al. (2009), who suggested a 20 wt% contribution from a chondritic impactor, but overlaps with the estimate of Ray et al. (2017), who have suggested a 6 wt% contribution from an EH-type chondritic impactor to the Lonar spherules. Based on Os concentrations and the $^{187}Os/^{188}Os$ ratio, a maximum contribution from a chondritic impactor of 0.03 wt % was estimated in the bulk impact glasses and melt rocks at Lonar (Schulz et al., 2016). The relatively low estimates of the impactor contribution in the bulk impactites compared to the spherules reflect the complex distribution mechanism of the impactor component in different impact-products, as also observed at other craters (cf., Goderis et al., 2013; Wittmann et al., 2013).

Although the Ir concentrations in the Lonar spherules are broadly similar (Fig. 4), the concentration ratios of MSE in the Lonar spherules show significant variability and overlap with published data for the Lonar spherules (Misra et al., 2009; Ray et al., 2017) (Fig. 7). Among the Lonar spherules, only the Group 1a and Group 2 show high Ni, Cr, EF_{Ni} and EF_{Cr} and higher Ni/Co, Cr/Co and Ni/Cr compared to the target basalts (Figs. 3c and 7). In contrast, the Group 1b spherules show significantly lower Cr, Co, and Ni concentrations (Table 2) and EF_{Cr} and EF_{Ni} values close to unity that overlap with those of the impact breccia (Fig. 3c). The Ni/Co, Ni/Cr and Fe/Cr values of the Group 1b spherules also overlap with those of the impact breccia and do not show any contribution from a chondritic source (Fig. 7). As discussed in the following section, the Group 1b spherule compositions appear to reflect contributions from the basement underlying the Deccan basalts.

4.5. Evidence for basement melting in the spherules and impact breccia at Lonar

The relatively radiogenic Sr and unradiogenic Nd isotopic composition as well as the high Rb/Sr and low Sm/Nd values of the impact breccia at Lonar have been explained by the melting and incorporation of the Precambrian basement beneath the Deccan basalts (Chakrabarti and Basu, 2006; Chakrabarti et al., 2006). A similar conclusion has been reached by Schulz et al. (2016) based on a combined Nd and Sr isotopic study of bulk impactites from Lonar, additionally supported by Os isotopic data on the same samples. It has been argued that some of the basaltic melts/glasses around Lonar might be of anthropogenic origin (Misra et al., 2009; Ray et al., 2017). Hence, in addition to impact breccia samples, we have analyzed non-spherical impact glasses as well as spherules in this study, the latter samples having a definitive impact cratering origin.

To investigate the melting of the basement and its incorporation in the Lonar impactites, we focus primarily on the variability of fluid immobile lithophile element concentrations and Nd and Sr isotope ratios. The varying lithologies and compositions of crustal xenoliths in the Deccan basalts,

ranging from augen gneiss to metamorphosed carbonates, highlight the heterogeneous nature of the basement (Ray et al., 2008). In the absence of any exposed basement samples at Lonar, the geochemical and isotopic composition of the Precambrian basement is estimated using data available for the average UCC (McLennan, 2001), granitic rocks from the Dharwar craton (Peucat et al., 1989) and crustal xenoliths BXAG and BXMC (Ray et al., 2008).

The Group 1b and Group 2 spherules show high EF_{Th} and trend (although weakly) towards EF_{Th} values of the UCC and BXMC (Fig. 3d). The Group 1b spherules also show higher EF_{Pb} trending towards the values for the UCC (Fig. 3f), both suggesting contribution of basement material to these spherules. In addition, the Group 1b spherules show higher LREE fractionation ($La/Sm_{(N)} = 1.51–1.94$) compared to the target basalts ($La/Sm_{(N)} = 1.27–1.57$) and overlap with that of the impact breccia ($La/Sm_{(N)} = 1.52–1.88$) (Table 1 and 2, Fig. 5a). Fractionation of LREE is unlikely to have occurred due to evaporation/condensation following impact as the REEs are refractory elements (50% $T_C = 1356–1659$ K; Lodders, 2003) and show geochemically coherent behaviour (cf., Rollinson, 1993). Consequently, LREE fractionation is likely to reflect melting and incorporation of the basement, which is expected to have higher $La/Sm_{(N)}$ (Figs. 5a, 7c). In addition to higher $La/Sm_{(N)}$, the Group 1b spherules show relative enrichments in Rb, Ba, Th, U and no depletion in Pb, similar to the UCC, BXAG and BXMC (Fig. 5b), consistent with basement melting. Another striking feature of the Group 1b spherules is the presence of negative Nb and Ta anomalies, similar to UCC, BXAG and BXMC, which are not observed in any of the other samples at Lonar (Fig. 5b). The negative Nb and Ta anomalies together with the lack of any negative Zr or Hf anomalies in the Group 1b spherules is also consistent with significant contributions from the basement to these samples. Interestingly, the Group 1b spherules show the lowest EF_{Ni} and EF_{Cr} (Fig. 3c), Ni/Co and Ni/Cr (Fig. 7a and b) among the spherules, although their Ir concentrations are comparable (Fig. 4). The above-mentioned geochemical characteristics of the Group 1b spherules and their overall compositional similarity with the impact breccia samples suggests that these spherules were formed primarily by mixing of basaltic as well as basement melts with some contribution of the impactor to explain the high Ir. The present study demonstrates that the basement melting signatures at Lonar are also preserved in the smallest and irrefutable products of impact cratering, i.e., impact spherules.

The impact breccia samples analyzed in this study show more radiogenic $^{87}Sr/^{86}Sr$ and less radiogenic $^{143}Nd/^{144}Nd$ compared to the target basalts (Fig. 6a), consistent with the results of Chakrabarti and Basu (2006) and Schulz et al. (2016) and the basement melting hypothesis (Chakrabarti and Basu, 2006). The Sr isotopic composition of spherules and non-spherical impact glasses as analyzed in this study show values that are somewhat in between (and partly overlapping with) the basalts and the impact breccia. However, the Nd isotopic composition of the non-spherical impact glasses, also irrefutable products of impact cratering given their aerodynamic shapes (Fig. 1c), show the most unradiogenic Nd isotopic composition among all the samples from Lonar (Fig. 6), providing further support for the basement melting hypothesis of Chakrabarti and Basu (2006).

The possibility of basement melting at Lonar hinges on the thickness of the Deccan basalts at Lonar and the depth of the Lonar crater. Depth estimates for the Lonar crater vary from 230 to 245 m (Fudali et al., 1980) to 150–300 m (Son and Koeberl, 2007). Based on numerical models, the depth of a simple crater is considered to be 0.2–0.33 times its diameter (Melosh, 1989). Using this relationship, the depth of the transient Lonar crater was estimated between 350 and 610 m (Chakrabarti and Basu, 2006). The latter depth estimate for the Lonar crater is more than the thickness of the Deccan basalts (~340 m), estimated from drill hole studies near Killari, which is located south of Lonar, in the eastern fringe of the Deccan traps (Gupta et al., 1999). While the exact thickness of the Deccan basalts at Lonar is not known, the depth estimates of the Lonar crater and the thickness of the Deccan basalts from the eastern part of the Deccan Traps are consistent with our geochemical and isotopic data for the Lonar crater basalts and impactites, which suggest that the basement beneath the Deccan basalts melted upon impact at Lonar.

The contribution of the basement melt to the Lonar impact breccia and non-spherical impact glasses can be estimated using two component mixing models between the basalts at Lonar and representative samples of the basement. Our first approach is based on the use of the Nd isotopic compositions as well as Nd concentrations of the end-members. Compositions of the basalt are taken from the present study while for the basement, we use data reported for granitic rocks from the Dharwar craton (Peucat et al., 1989), for which Nd isotopic data are available. Neodymium isotopic data has not been reported for the basement xenoliths BXAG and BXMC (Ray et al., 2008). The average Nd concentration of the Lonar basalts is 21.2 ppm whereas the average $^{143}Nd/^{144}Nd$ ratio is 0.512701. The average Nd concentration of the granitic gneiss samples 6610, 6611, 6612, and 6615 (Peucat et al., 1989) is 15.6 ppm whereas the average $^{143}Nd/^{144}Nd$ ratio of the above-mentioned samples is 0.510579. Our calculations suggest that the ranges of $^{143}Nd/^{144}Nd$ ratios observed in the Lonar impact breccia and non-spherical impact glasses require between 6 and 27 wt% contribution of the basement. These calculations are sensitive to the Nd concentrations of the end-members. While the Lonar basalts show a limited spread in their Nd concentrations, the granitic gneiss samples show a large range in Nd from 2.2 to 34.6 ppm. If we consider only sample 6610 with the highest Nd concentration (34.6 ppm) as representative of the basement, the compositions of the impact breccia and non-spherical impact glasses require up to 15 wt% contribution of the basement. This estimate is closer to estimates based on Sr isotope ratios.

The Sr concentration and $^{87}Sr/^{86}Sr$ of the average Lonar basalt is 221 ppm and 0.706427, respectively. Strontium isotopic data are available for the granitic gneiss samples (Peucat et al., 1989) as well as the augen gneiss (BXAG) and meta-carbonate (BXMC) xenoliths (Ray et al., 2008).

The Sr concentrations of the average granitic gneiss, BXAG, and BXMC are 546 ppm, 284 ppm and 1025 ppm, respectively, whereas their corresponding $^{87}Sr/^{86}Sr$ ratios are 0.719555, 0.72801, and 0.70935. Our calculations suggest that basement rocks akin to the augen gneiss or the Dharwar granites contribute 2–4 wt% to the compositions of the spherules and 4–8 wt% to the compositions of the non-spherical impact glasses and impact breccia (Fig. 6b). However, the Sr isotopic composition of the Lonar impactites cannot be explained by mixing with a pure meta-carbonate basement with a BXMC-like composition (Fig. 6b). The discrepancy between the basement contribution estimates in the impact breccia and non-spherical impact glasses using Nd isotope ratios versus Sr isotope ratios is most likely due to the heterogeneous composition of the basement, as observed in the basement xenoliths (Ray et al., 2008). Our estimates of the basement contribution are thus consistent with the <15 wt% contribution estimate of Schulz et al. (2016), also based on the Sr and Nd isotopic compositions of bulk Lonar impactites.

4.6. Evidence of impact volatilization and re-condensation and melt-chondrite mixing in the spherules

Impact cratering involves fracturing, melting of the target rock and vaporization of the impactor as well as the target rock. Geochemical and isotopic studies of impact rocks provide a better understanding of the complex interplay of the above processes. To study the possibility of elemental fractionation due to evaporation upon impact and subsequent condensation, we studied the variations of volatile element concentrations in the Lonar impactites. Zinc (50% T_C of 726 K) and Pb (50% T_C of 727 K) have similar volatility and are more volatile compared to Na (50% T_C of 958 K), K (50% T_C of 1006 K) and Cu (50% T_C of 1037 K) (Lodders, 2003).

Low concentrations of Na in Lonar impact glasses were suggested to result from impact-induced volatile losses (Fredriksson et al., 1973; Stroube et al., 1978). The relatively low EF_{Na}, EF_K as well as EF_{Pb} in the unaltered Group 1a spherules of this study and their positive correlations with EF_{Zn} (Fig. 3f, g, h) could reflect volatile loss upon impact. However, Pb, Na and K are also fluid mobile, whereas Cu and Zn are relatively fluid immobile. The Group 1a and Group 2 spherules show correlated EF_{Zn} and EF_{Cu} variations (Fig. 3e) and large variations in Zn and Cu concentrations (Fig. 8). These variations do not show any clear mixing trends between the basalts, chondrites, and the basement (UCC, BXAG, BXMC) (Fig. 8). Some spherules show Zn and Cu concentrations that are even higher than the above-mentioned end-members. The overall Cu and Zn concentrations in the Lonar spherules are significantly higher than the average concentrations reported in tektites from all major strewn fields (Ivory Coast, Australasian, Central European, North American) (Moynier et al., 2009, 2010) (Fig. 8) and overlap with the concentrations reported earlier for Lonar spherules (Misra et al., 2009; Ray et al., 2017) and Lonar impact glasses (Son and Koeberl, 2007). While the depletions in Zn observed in some of the spherules relative to the basalts (Fig. 8) can be explained due to volatile loss upon impact, the enrichments in Zn in some of the spherules require a different explanation.

One possibility is that the high Cu and Zn concentrations in the Lonar spherules result from mixing with Cu and Zn-bearing sulfides, which could be present in the basement. However, the occurrence of such sulfides beneath the Deccan basalts is merely speculative. Zinc-bearing sulfides are also expected to be enriched in Pb owing to their similar chalcophilic behaviour. The moderate positive correlation between EF_{Pb} and EF_{Zn} in the Group 1a spherules ($R^2 = 0.68$) (Fig. 3f) is consistent with the sulfide admixture hypothesis. However, most of the Group 1a spherules show negative Pb anomalies (Fig. 5b), which is inconsistent with mixing with sulfide-rich rocks, as mixing with sulfides would have enriched the spherules in Pb. In addition, the moderate positive correlation between EF_K and EF_{Zn} ($R^2 = 0.70$) (Fig. 3g) as well as EF_{Na} and EF_{Zn} ($R^2 = 0.62$) in the Group 1a spherules rules out the contribution of sulfides, as sulfides do not contain any significant amounts of K or Na. The impact breccia samples at Lonar, which show clear isotopic and geochemical evidence for melting of basement rocks, do not show any enrichment in Zn and Cu, opposed to the spherules (Fig. 8). Overall, the above observations suggest a volatility-driven mechanism to explain the Zn and Cu enrichment in the Lonar spherules.

Stable isotope ratios of Cu and Zn have been shown to fractionate during impact cratering; tektites are depleted in the lighter isotopes of Cu and Zn, which are preferentially volatilized during impact (Moynier et al., 2009, 2010). Previously characterized Lonar impact glass samples (Son and Koeberl, 2007) (labelled type x and y, Fig. 8), which mostly exhibit higher Zn concentrations compared to the basalts, were analyzed for their Zn isotopic compositions by Moynier et al. (2008). The $\delta^{66/64}Zn$ of the x-type glasses are relatively low and range between −0.39 and −0.3‰ while the $\delta^{66/64}Zn$ for the y-type glasses range from 0 to +0.4‰.

Tektites (distal ejecta) from different parts of the world are typically depleted in the lighter isotopes of Zn and this depletion is explained by evaporation in a diffusion-limited regime (Moynier et al., 2009). A Rayleigh distillation model predicts that the volatile loss of Zn is accompanied by loss of lighter isotopes of Zn (Moynier et al., 2009). To satisfy mass balance considerations, the lighter isotopes of Zn should be enriched in a complementary reservoir (condensate), which is also expected to be enriched in Zn concentrations. This volatile-enriched component is expected to be found at the periphery of the ejecta plume where temperatures are lower.

The x-type impact glasses from Lonar are anomalously enriched in the lighter isotopes of Zn (Moynier et al., 2008). The high Zn (and Cu) concentrations in the Lonar spherules, along with the enrichment in lighter isotopes of Zn in the Lonar x-type impact glasses are best explained by condensation from a volatile-enriched vapour condensate. This volatile-enriched component is uniquely preserved at the Lonar crater. Since all spherules of this study were collected from the same location (Fig. 1a), the

preservation of the volatile-enriched component does not have any lateral spatial significance and is best explained by geochemical and isotopic fractionation in a vertical direction within the vapour cloud. The impact spherules that experienced volatile loss were possibly carried to greater vertical distances and these condensates eventually landed in the same place as the other spherules, which traversed less vertical distances.

5. CONCLUSIONS

This study reports major and trace element concentrations of 9 target basalts, 7 impact breccia, a red bole, non-spherical impact glasses using solution-based ICPMS and 35 sub-mm sized spherules using LA-ICPMS from the Lonar crater. We also report Nd and Sr isotopic compositions of selected samples.

(1) The chemical index of alteration (CIA) of the impact breccia and majority of the spherules (Group 1) at the Lonar crater shows overall low values suggesting minimal aqueous alteration in these samples. Seven spherules show significantly higher CIA (Group 2), which overlap with that of the red bole, a product of basalt weathering. Therefore, CIA values may be used to screen impactites for late-stage aqueous alteration.
(2) The trace element and Nd and Sr isotopic compositions rule out any significant contribution of the red bole-type weathered material to the composition of the impactites at Lonar crater.
(3) The MSE ratios in the Lonar spherules rule out contributions from an iron meteoritic as well as achondritic impactors and agree with a chondritic impactor at Lonar. Significantly elevated Ir concentrations compared to the target basalt in some spherules, along with high Cr concentrations in the same samples, suggest contributions of up to 8 wt% of a chondritic impactor in the Lonar impactites. The meteoritic contribution is particularly prominent in the Group 1a (higher Ni than Group 1b) spherules and in the Group 2 spherules.
(4) The relatively radiogenic Sr and unradiogenic Nd isotopic compositions of the Lonar impact breccia are consistent with melting of the Precambrian basement upon impact at Lonar. Two component mixing calculations between the target basalts and samples representative of the basement suggest less than 15 wt% contribution of the basement to the Lonar impactites. The considerable LREE fractionation, high enrichments in Rb, Ba, Th and U relative to the target basalts, lack of depletion in Pb, presence of negative Nb and Ta anomalies in the Group 1b spherules and their overall geochemical similarity to the impact breccia suggests contributions from the basement to the compositions of these spherules. The basement contribution is between 2 and 4 wt% for the spherules and highest (~15 wt%) for the non-spherical impact glasses. The present study demonstrates that the basement melting signatures at Lonar are also preserved in the smallest and irrefutable products of impact cratering, i.e., the spherules.
(5) The variability in the moderately siderophile element ratios (Ni/Co, Cr/Co, Ni/Cr, Fe/Cr) as well as La/$Sm_{(N)}$ values of the spherules and impact breccia at Lonar crater require mixing between three end-members: the target basalts, a chondritic impactor and the basement underlying the Deccan basalts.
(6) Geochemical variations of non-fluid mobile volatile elements in the Lonar spherules reflect evaporation-condensation effects accompanying the impact cratering event. While some spherules show depletions in Zn and Cu, consistent with volatile loss, several spherules show enrichments in these volatile elements. The enrichments in Zn and Cu in the spherules are best explained by condensation from a volatile-enriched vapour condensate and reflect geochemical and isotopic fractionation in a vertical direction within the vapour cloud.
(7) This study highlights the importance of spherules, the sub-mm sized products of impact cratering, the compositions of which can not only record the projectile contribution to basaltic targets, but also the complex interplay of melting, mixing and evaporation-condensation processes during an impact event.

ACKNOWLEDGEMENTS

This work was funded by ISRO-STC (ISTC/EES/RC/304) to RC. We thank Mr. Ratikanta Sikdar for his help during fieldwork at Lonar. RC thanks Sarah T. Stewart for discussions on impact volatilization. Part of this work is supported by VUB Strategic Research. SG is a Postdoctoral Fellow of the Research Foundation - Flanders (FWO). We thank two anonymous reviewers and the Associate Editor Dr. Christian Koeberl for their valuable comments and suggestions.

APPENDIX A. SUPPLEMENTARY MATERIAL

Supplementary data associated with this article can be found, in the online version, at http://dx.doi.org/10.1016/j.gca.2017.07.022.

REFERENCES

Banerjee A., Chakrabarti R. and Mandal S. (2016) Geochemical anatomy of a spheroidally weathered diabase. *Chem. Geol.* **440**, 124–138.

Chakrabarti R. and Basu A. R. (2006) Trace element and isotopic evidence for Archean basement in the Lonar crater impact breccia, Deccan Volcanic Province. *Earth. Planet. Sci. Lett.* **247** (3), 197–211.

Chakrabarti R., Basu A. R. and Ghatak A. (2006) Reply to, Comments on "Trace element and isotopic evidence for Archean basement in the Lonar crater impact breccia, Deccan volcanic province" by Ramananda Chakrabarti and Asish R. Basu. *Earth. Planet. Sci. Lett.* **250**(3), 669–670.

Crocket J. H. and Paul D. K. (2004) Platinum-group elements in Deccan mafic rocks, a comparison of suites differentiated by Ir content. *Chem. Geol.* **208**(1–4), 273–291.

Deenadayalan K., Basavaiah N., Misra S. and Newsom H. (2009) Absence of Archean Basement in the Genesis of Lonar Crater, India. *72nd Annual Meteoritical Society Meeting*, #5388(abstr.).

Evans N. J., Gregoire D. and Goodfellow W. (1993) Use of platinum-group elements for impactor identification: Terrestrial impact craters and Cretaceous-Tertiary boundary. *Geochim. Cosmochim. Acta* **57**(15), 3737–3748.

Feldman V., Sazonova L., Mironov Y.V., Kapustkina I. and Ivanov B. (1983) Circular structure Logancha as possible meteorite crater in basalts of the Tunguska syneclise. *Lunar Planet. Sci. XIV*. #1098(abstr.).

Fredriksson K., Dube A., Milton D. and Balasundaram M. (1973) Lonar Lake, India: an impact crater in basalt. *Science* **180** (4088), 862–864.

Fudali R. and Fredriksson K. (1992) Tektite-like bodies at Lonar Crater, India? Very unlikely. *Meteoritics* **27**(1), 99–100.

Fudali R., Milton D., Fredriksson K. and Dube A. (1980) Morphology of Lonar crater, India: comparisons and implications. *Moon Planets* **23**(4), 493–515.

Gaillardet J., Dupre B., Louvat P. and Allegre C. J. (1999) Global silicate weathering and CO_2 consumption rates deduced from the chemistry of large rivers. *Chem. Geol.* **159**(1–4), 3–30.

Gilbert G. K. (1896) The origin of hypotheses, illustrated by the discussion of a topographic problem. *Science* **3**(53), 1–13.

Goderis S., Paquay F. and Claeys P. (2012) Projectile identification in terrestrial impact structures and ejecta material. In *Impact cratering: Processes and Products* (eds. G. R. Osinski and E. Pierazzo). Wiley Blackwell, pp. 223–239.

Goderis S., Wittmann A., Zaiss J., Elburg M., Ravizza G., Vanhaecke F., Deutsch A. and Claeys P. (2013) Testing the ureilite projectile hypothesis for the El'gygytgyn impact: determination of siderophile element abundances and Os isotope ratios in ICDP drill core samples and melt rocks. *Meteorit. Planet. Sci.* **48**(7), 1296–1324.

Gupta H. K., Rao R. U. M., Srinivasan R., Rao G. V., Reddy G. K., Dwivedy K. K., Banerjee D. C., Mohanty R. and Satyasaradhi Y. R. (1999) Anatomy of surface rupture zones of two stable continental region earthquakes, 1967 Koyna and 1993 Latur, India. *Geophys. Res. Lett.* **26**(13), 1985–1988.

Hagerty J. J. and Newsom H. E. (2003) Hydrothermal alteration at the Lonar Lake impact structure, India: Implications for impact cratering on Mars. *Meteorit. Planet. Sci.* **38**(3), 365–381.

Hawkes H. (1967) Geochemical evidence on the origin of the Lonar Crater, Maharashtra, India: discussion. *Bull. Geol. Soc. Am.* **78** (9), 1199–1200.

Hecht L., Wittmann A., Schmitt R. T. and Stöffler D. (2004) Composition of impact melt particles and the effects of post-impact alteration in suevitic rocks at the Yaxcopoil-1 drill core, Chicxulub crater, Mexico. *Meteorit. Planet. Sci.* **39**(7), 1169–1186.

Jourdan F., Moynier F., Koeberl C. and Eroglu S. (2011) $^{40}Ar/^{39}Ar$ age of the Lonar crater and consequence for the geochronology of planetary impacts. *Geology* **39**(7), 671–674.

Kallemeyn G. W. and Wasson J. T. (1985) The compositional classification of chondrites: IV. Ungrouped chondritic meteorites and clasts. *Geochim. Cosmochim. Acta* **49**, 261–270.

Kieffer S. W., Schaal R. B., Gibbons R., Horz R., Milton D. J. and Dube A. (1976). Shocked basalt from Lonar impact crater, India, and experimental analogues. *Proc. 7th Lunar Planet. Sci. Conf.* pp. 1391–1412.

Koeberl C. (1998) Identification of meteoritic components in impactites. *Geol. Soc., Lond., Spec. Publ.* **140**(1), 133–153.

Koeberl C. (2002) Mineralogical and geochemical aspects of impact craters. *Mineral. Mag.* **66**(5), 745–768.

Koeberl C., Claeys P., Hecht L. and McDonald I. (2012) Geochemistry of impactites. *Elements* **8**(1), 37–42.

Koeberl C., Mougel B. and Moynier F. (2017) Meteoritic component from the Boltysh (Ukraine) and Lonar (India) Impact Structures: First Assessment. *Lunar Planet. Sci. XLVIII*. #1331 (abstr.).

La Touche T. and Christie W. (1912) The geology of the Lonar Lake. *Rec. Geol. Survey India* **41**, 266–275.

Lafond E. C. and Dietz R. S. (1964) Lonar Crater, India, a meteorite crater? *Meteoritics* **2**(2), 111–116.

Lodders K. (2003) Solar system abundances and condensation temperatures of the elements. *Astrophys. J.* **591**(2), 1220–1247.

Maloof A. C., Stewart S. T., Weiss B. P., Soule S. A., Swanson-Hysell N. L., Louzada K. L., Garrick-Bethell I. and Poussart P. M. (2010) Geology of Lonar Crater, India. *Bull. Geol. Soc. Am.* **122**(1–2), 109–126.

Masaitis V. (1999) Impact structures of northeastern Eurasia, The territories of Russia and adjacent countries. *Meteorit. Planet. Sci.* **34**(5), 691–711.

Mason B. (Ed.), (1979) Chapter B. Cosmochemistry. *Data of Geochemistry*. United States Government Printing Office, Washington D.C., pp. B1–B132.

Master S. (1999) Evidence for an impact origin of the Ambar Lake structure, A smaller companion crater to the Lonar impact crater, Maharashtra, India. *Meteorit. Planet. Sci. Supplement.* **34**(4), A78.

McLennan S.M. (2001) Relationships between the trace element composition of sedimentary rocks and upper continental crust. *Geochem. Geophys. Geosys.* **2(4)**, ISSN 1525-2027.

Melosh H. J. (1989) *Impact Cratering: A Geologic Process*. Oxford University Press, New York (Oxford Monographs on Geology and Geophysics, No. 11).

Misra S. (2006) Comments on, "Trace element and isotopic evidence for Archean basement in the Lonar crater impact breccia, Deccan volcanic province" by Ramananda Chakrabarti and Asish R. Basu in Earth. Planet. Sci. Lett. 247 (2006) 197–211. *Earth. Planet. Sci. Lett.* **250(3)**, 667–668.

Misra S. and Newsom H.E. (2011) Incompatible Trace Element Fractionation in Impact-Melts of Lonar Crater, India - Evidence of Differential Impact Melting of Target Deccan Basalt, *Lunar Planet. Sci. XLII*. #1060(abstr.).

Misra S., Newsom H. E., Prasad M. S., Geissman J. W., Dube A. and Sengupta D. (2009) Geochemical identification of impactor for Lonar crater, India. *Meteorit. Planet. Sci.* **44**(7), 1001–1018.

Morgan J. (1978) Lonar crater glasses and high-magnesium australites-Trace element volatilization and meteoritic contamination. *Proc. 9th Lunar Planet. Sci. Conf.*, pp. 2713–2730.

Moynier F., Jourdan F., Yin Q-z., Beck P., Koeberl C. and Reimold U. (2008) Isotopic fractionation of Zn during impact on Earth. *Lunar Planet. Sci. XXXIX*. #1426(abstr.).

Moynier F., Beck P., Jourdan F., Q-z Yin., Reimold U. and Koeberl C. (2009) Isotopic fractionation of zinc in tektites. *Earth. Planet. Sci. Lett.* **277**(3), 482–489.

Moynier F., Koeberl C., Beck P., Jourdan F. and Telouk P. (2010) Isotopic fractionation of Cu in tektites. *Geochim. Cosmochim. Acta* **74**(2), 799–807.

Murali A., Zolensky M. and Blanchard D. (1987) Tektite-like bodies at Lonar Crater, India: Implications for the origin of tektites. J. Geophys. *Res.: Solid Earth* **92**(B4).

Nandy N. and Deo V. (1961) Origin of the Lonar lake and its alkalinity. *TISCO* **8**(3), 1–12.

Nayak V. (1972) Glassy objects (impactite glasses?) A possible new evidence for meteoritic origin of the Lonar crater, Maharashtra State, India. *Earth. Planet. Sci. Lett.* **14**(1), 1–6.

Nesbitt H. W. and Young G. M. (1982) Early Proterozoic climates and plate motions inferred from major element chemistry of lutites. *Nature* **299**(5885), 715–717.

Osae S., Misra S., Koeberl C., Sengupta D. and Ghosh S. (2005) Target rocks, impact glasses, and melt rocks from the Lonar impact crater, India: Petrography and geochemistry. *Meteorit. Planet. Sci.* **40**(9/10), 1473–1492.

Palme H., Janssens M.-J., Takahashi H., Anders E. and Hertogen J. (1978) Meteoritic material at five large impact craters. *Geochim. Cosmochim. Acta* **42**(3), 313–323.

Peucat J. J., Vidal P., Bernard-Griffiths J. and Condie K. C. (1989) Sr, Nd, and Pb isotopic systematics in the archean low-grade to high-grade transition zone of Southern India: syn-Accretion Vs post-accretion granulites. *J. Geol.* **97**(5), 537–549.

Peucker-Ehrenbrink B. and Jahn B.M. (2001) Rhenium-osmium isotope systematics and platinum group element concentrations: Loess and the upper continental crust. *Geochem. Geophys. Geosys.* **2**(**10**), ISSN 1525-2027.

Ray D., Upadhyay D., Misra S., Newsom H. E. and Ghosh S. (2017) New insights on petrography and geochemistry of impactites from the Lonar crater, India. *Meteorit. Planet. Sci.*. http://dx.doi.org/10.1111/maps.12881.

Ray R., Shukla A. D., Sheth H. C., Ray J. S., Duraiswami R. A., Vanderkluysen L., Rautela C. S. and Mallik J. (2008) Highly heterogeneous Precambrian basement under the central Deccan Traps, India: direct evidence from xenoliths in dykes. *Gondwana Res.* **13**(3), 375–385.

Rehkamper M., Halliday A. N., Fitton J. G., Lee D. C., Wieneke M. and Arndt N. T. (1999) Ir, Ru, Pt, and Pd in basalts and komatiites: new constraints for the geochemical behavior of the platinum-group elements in the mantle. *Geochim. Cosmochim. Acta* **63**(22), 3915–3934.

Rollinson H. (1993) *Using geochemical data, Evaluation, Presentation, Interpretation*. Longman Group, UK.

Rudnick R.L. and Gao S. (2003) Composition of the continental crust. In Treatise on Geochemistry, Vol. 1 Meteorites, Comets and Planets (eds. A.M. Davis and H.D. Holland). Elsevier, vol. 3, pp. 593–659.

Schulz T., Luguet A., Wegner W., van Acken D. and Koeberl C. (2016) Target rocks, impact glasses, and melt rocks from the Lonar crater, India: highly siderophile element systematics and Sr-Nd-Os isotopic signatures. *Meteorit. Planet. Sci.* **51**(7), 1323–1339.

Sengupta D., Bhandari N. and Watanabe S. (1997) Formation age of Lonar meteor crater, India. *Revista de Fisica Aplicada e Instrumentacao* **12**(1), 1–7.

Son T. H. and Koeberl C. (2007) Chemical variation in Lonar impact glasses and impactites. *GFF* **129**(2), 161–176.

Storzer D. and Koeberl C. (2004) Age of the Lonar impact crater, India: First results from fission track dating. *Lunar Planet. Sci. XXXV*. #1309(abstr.).

Stroube W., Garg A., Ali M. and Ehmann W. (1978) A chemical study of the impact glasses and basalts from Lonar Crater, India. *Meteoritics* **13**(2), 201–208.

Sun S.-s. and McDonough W. S. (1989) Chemical and isotopic systematics of oceanic basalts: implications for mantle composition and processes. *Geol. Soc., Lond., Spec. Publ.* **42**(1), 313–345.

Tagle R. and Berlin J. (2008) A database of chondrite analyses including platinum group elements, Ni Co, Au, and Cr: implications for the identification of chondritic projectiles. *Meteorit. Planet. Sci.* **43**(3), 541–559.

Tagle R. and Hecht L. (2006) Geochemical identification of projectiles in impact rocks. *Meteorit. Planet. Sci.* **41**(11), 1721–1735.

Taylor S. R. and McLennan S. M. (1985) *The Continental Crust: Its Composition and Evolution*. Blackwell Scientific Pub, Palo Alto, CA.

Van Roosbroek N., Debaille V., Pittarello L., Goderis S., Humayun M., Hecht L., Jourdan F., Spicuzza M. J., Vanhaecke F. and Claeys P. (2015) The formation of IIE iron meteorites investigated by the chondrule-bearing Mont Dieu meteorite. *Meteorit. Planet. Sci.* **50**(7), 1173–1196.

Venkatesh V. (1965) Geochemical evidence for the origin of the Lonar Crater, Maharashtra, India. *Bull. Geol. Soc. Am.* **76**(11), 1315–1316.

Walker D., Stolper E. and Hays J. (1979) Basaltic volcanism: The importance of planet size. *Proc. 10th Lunar Planet. Sci. Conf.*, pp. 1995–2015.

Wilkins A., Subbarao K. V., Ingram I. and Walsh J. N. (1994) Weathering regimes within the Deccan Basalts. In *Volcanism* (ed. K. V. Subbarao). Wiley, New Delhi, pp. 217–232.

Wittmann A., Goderis S., Claeys P., Vanhaecke F., Deutsch A. and Adolph L. (2013) Petrology of impactites from El'gygytgyn crater, Breccias in ICDP-drill core 1C, glassy impact melt rocks and spherules. *Meteorit. Planet. Sci.* **48**(7), 1199–1235.

Associate editor: Christian Koeberl